2-1-2012

Microwave Interferometer and Refractometer for the WB-8 Polywell Fusion Device

Kevin Davis

Follow this and additional works at: https://digitalrepository.unm.edu/ece_etds
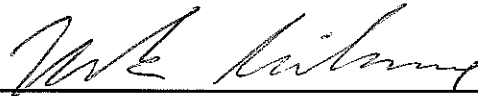
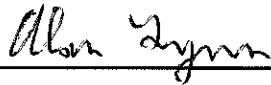# Kevin Davis

Candidate

Electrical Engineering
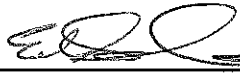
Department

This thesis is approved, and it is acceptable in quality and form for publication:

Approved by the Thesis Committee:

_____ , Chairperson

_____

_____

_____

_____

_____

_____

**MICROWAVE INTERFEROMETER AND
REFRACTOMETER
FOR THE WB-8 POLYWELL FUSION DEVICE**

by

KEVIN DAVIS

**B.S., ELECTRICAL AND COMPUTER ENGINEERING,
UNIVERSITY OF COLORADO, 2004**

THESIS

Submitted in Partial Fulfillment of the
Requirements for the Degree of

M.S., Electrical Engineering

The University of New Mexico
Albuquerque, New Mexico

December, 2011

DEDICATION

to

Kourtney Davis

I am still fighting to deserve you.

ACKNOWLEDGEMENTS

I owe nearly all the knowledge and experience I gained on this project to my advisor, Dr. Mark Gilmore. But more than the time and teaching, which you were generous with, I can't thank you enough for the faith you showed in me by bringing me onto this project.

Thanks to Dr. Alan Lynn and Dr. Edl Schamiloglu for being on my committee. Dr Lynn was a tremendous help as I began working on this project, particularly as I learned how to think about the optics. I appreciate you both for your time and your experience.

In addition, I must thank Dr. Jaeyoung Park for not only his role in funding the project, but also for providing a great deal of guidance. With Dr. Gilmore and Dr. Park overseeing my work I was in a great position to succeed.

My amazing parents, Kevin and Christine Davis, have provided a limitless supply of everything I've ever needed. Their names belong by anything I ever accomplish. The added support of my wife's parents, Kevin and Nancy Leaderer, has meant more than they know.

Finally, thank you Dr. Jamesina Simpson. You were right. It was a good idea to go back to school.

MICROWAVE INTERFEROMETER AND REFRACTOMETER FOR THE WB-8 POLYWELL FUSION DEVICE

by

Kevin M. Davis

B.S., Electrical and Computer Engineering, University of Colorado, 2004

M.S., Electrical Engineering, University of New Mexico, 2011

ABSTRACT

The WB-8 chamber is an inertial electrostatic confinement device which is being tested by Energy Matter Conversion Corporation in an attempt to study the viability of their Polywell design as a source of fusion energy.   One of the primary diagnostic tools will be a 94 GHz interferometer which will give a line average density measurement of a chord through the plasma. The rate at which ions take part in a fusion event depends heavily on the density, making the interferometer measurements vital in assessing the progress made with WB-8.

In order to take density measurements, a beam must pass through the plasma and be collected on the other end. One of the challenges in building an interferometer is designing lenses that can transmit a suitable beam into the test chamber. The beam

leaving a horn antenna is approximately Gaussian. Using Gaussian optics a lens can be used to focus the beam in order to probe the center of the plasma and provide sufficient energy at the receiver.

While the interferometer provides an average density, a more thorough picture of the density profile is needed to have a good understanding of how well the Polywell is functioning. A refractometer is also being built which will transmit a beam similar to that sent by the interferometer. This second beam, with a frequency of 136 GHz, is aimed parallel to the interferometer. Instead of propagating through the center of the plasma, the refractometer beam will have a translating launch point which can probe the plasma through different chords. By detecting the shape and location of the beam at the receiving end of the chamber the hope is that we will have additional information about the density profile.

TABLE OF CONTENTS

LIST OF FIGURES

LIST OF FIGURES

1. WB-8

Energy Matter Conversion Corporation has spent more than 25 years studying the viability of their Polywell fusion device as a potential energy source. The design differs from other fusion containment schemes in that the plasma is controlled by a static electric field. Building on the Farnsworth-Hirsch Fusor and the Elmore-Tuck-Watson Fusor, the Polywell replaces the charged grids in those devices, which became the main sources of loss, with a magnetic field intended to concentrate electrons at the center of the plasma [*Bussard*].

Fusion energy is created at a rate proportional to the density of the fuel squared. By focusing the electrons in center of the plasma, a virtual anode is created which in turn pulls ions to the center. Figure 1-1 shows a plot of the intended potential along a chord through the center
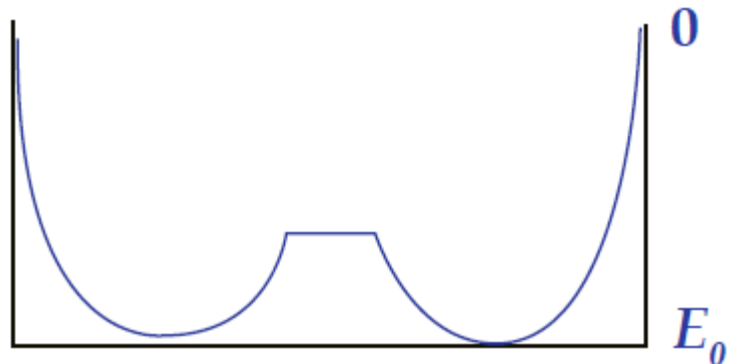
Figure 1-1: Electric potential at the center of the Polywell chamber. *[Bussard]*

of the plasma. Concentrating ions in the center of the plasma greatly increases the density of the fuel which in turn increases the frequency of fusion events.[*Chen*] In spite what may seem to be the case based on the plot of potential, the plasma remains approximately neutral.

In addition to increasing the rate of fusion, inertial electrostatic confinement (IEC) devices like the Polywell aim to prevent charged particles from

Figure 1-2: Coils used to create the confining magnetic field. *[Bussard]*

escaping from the system. The virtual anode in the center will hold the ions, which will oscillate around the center until being part of a fusion event. Electrons are contained by the magnetic field. Figure 1-2 shows the arrangement of coils used to create the desired magnetic field while Figure 1-3 shows the intended magnetic field in the plasma where magnetic mirror effects keep the electrons from escaping. It is necessary to continue injecting electrons into the plasma as they can be lost through the cusps of the magnetic field. In an ideal picture, even electrons that escape through the cusps would follow the field lines back into the plasma. Only the products of fusion are intended to leave the system. It is advantageous that the Polywell decouples the challenges of containing ions and electrons.[*Bussard*]

Ions are introduced at the edge of the plasma with low energy. The energy required for fusion is built up as the ion falls into the well created by the electrons. Energy of
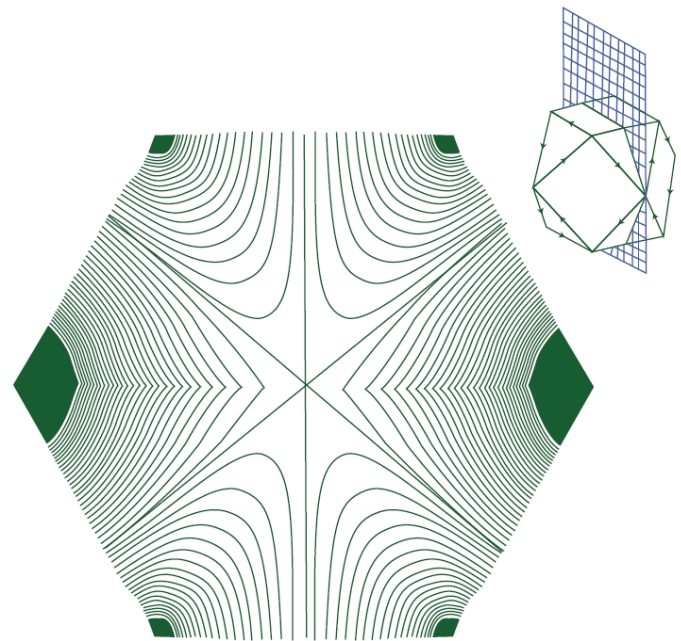
Figure 1-3: Magnetic field lines inside the Polywell *[Krall]*

2

the particles, along with density, is a primary limiting factor for fusion. In particular, the energy affects the cross-section, which is the probability of a fusion event. As energy increases, the cross section increases up to a maximum point before decreasing again.[Krall] Because the ion and electron containments are decoupled in a polywell device, it is easy to find the potential of the well that will lead to the desired energy in our ion species.

This leads to one of the arguments for the Polywell over other fusion devices. The peak cross-section of a tritium-deuterium fusion reaction occurs when both particles have an energy of ~40KeV. The neutron released in this reaction can lead to radioactive waste. This is the reaction that tokamaks attempt to achieve. There is hope that the Polywell can create a proton-Boron 11 fusion reaction. This reaction, which requires particles to reach ~560KeV, does not result in free neutrons, reducing the amount of waste produced.

The importance of plasma density to the success of a fusion device leads to the goal of this thesis. In the following chapter I discuss the interferometer, which will be used to measure the average density across a chord through the plasma. While that chapter focuses on the microwave circuitry, Chapter 3 discusses the optics used to create a beam which can probe the plasma. The final theory chapter discusses the design of our refractometer, with a goal of providing a more detailed picture of our plasma's density profile.

Bench testing data is presented in Chapter 5 where the actual behavior of the interferometer and refractometer are compared with the theory. The focus is on the optics where space constraints limited the size of lenses and mirrors. Chapter 6 shows

the interferometer data collected from WR-8 and how that data is converted to an average

density. In the conclusion, I give an update of WR-8 and discuss the remaining work

necessary to fully implement the refractometer.

2. Interferometer

Electromagnetic waves can be used to take measurements of a plasma when a physical probe is too intrusive or would be damaged by the high temperature environment. Interferometry uses interference between a wave passed through the plasma and a reference wave to find the refractive index of the plasma. Provided that the wave has a low enough energy and operates in a specific frequency range the effect on the plasma is negligible. The refractive index can then be used to find the average electron density over the region of the plasma that was sampled. This chapter will cover the selection of our interferometer design as well as the method of extracting a density measurement from our interferometer's output.

2.1 Frequency Selection

Depending on the direction of propagation and the applied magnetic field, waves at certain frequencies will not propagate. If it is possible to transmit the signal perpendicular to the applied magnetic field and the wave is polarized along **B** then it is referred to as an ordinary wave and has a dispersion relation given by

$$n_0^2 = 1 - \frac{\omega_p^2}{\omega^2} \qquad (2.1)$$

where

n_0 is the refractive index

ω is the frequency of the wave

ω_p is the plasma frequency [*Hutchinson*]

When the frequency of the wave is less than the plasma frequency the refractive index is imaginary and the wave will not propagate. The plasma frequency depends on the density of the plasma and is given by

$$\omega_p = \sqrt{\frac{n_e e^2}{\epsilon_0 m_e}} \qquad (2.2)$$

where

n_e is the electron plasma density

e is the charge of an electron

m_e is the mass of an electron

ϵ_0 is the permittivity of free space

Because the mass of an ion species is much higher than an electron, the ion plasma frequency is typically much smaller than the electron plasma frequency and the frequency of the transmitted wave. As a result the ion plasma frequency has a negligible effect on the dispersion relation.

The geometry of our system prevents us from launching the interferometer beam perpendicular to the applied magnetic field. Instead, the beam will be parallel to the applied field. In this case there are two types of waves to consider, left-handed and right-handed waves. The dispersion relations for these two types of waves are given by:

$$n_R^2 = 1 - \frac{\omega_{pi}^2}{\omega(\omega + \omega_{ci})} - \frac{\omega_{pe}^2}{\omega(\omega - \omega_{ce})} \qquad (2.3)$$

$$n_L^2 = 1 - \frac{\omega_{pi}^2}{\omega(\omega - \omega_{ci})} - \frac{\omega_{pe}^2}{\omega(\omega + \omega_{ce})} \qquad (2.4)$$

where

ω_{pi} is the plasma frequency for the ions

ω_{pe} is the plasma frequency for the electrons

ω_{ci} is the cyclotron frequency of the ions

ω_{ce} is the cyclotron frequency of the electrons [*Swanson*]
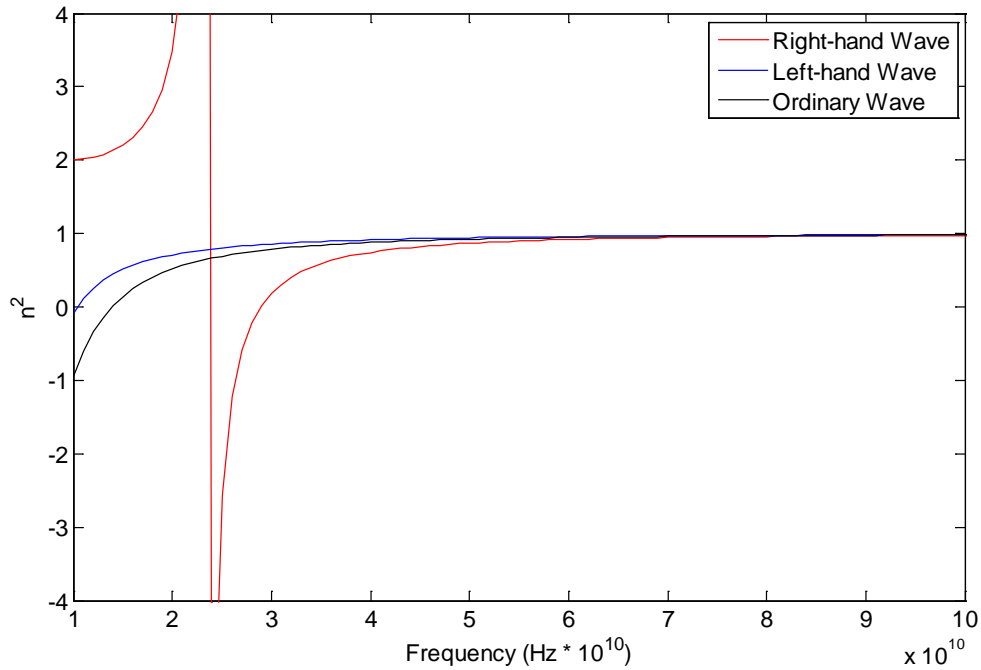
Figure 2-1: Dispersion relations for different wave modes in a plasma with a constant density of 2*10¹² cm⁻³

The cyclotron frequency is the angular frequency at which a particle circles a magnetic field line and is given by

$$\omega_c = \frac{qB}{m}$$

where

B is the magnetic field strength

m is the mass of the particle

q is the charge of the particle

While the ordinary wave has a simple cutoff frequency, left and right-handed waves have a more complicated region of propagation. Figure 2-1 shows a plot of the dispersion relations for each of these three waves in a plasma with a density of $2 *$ $10^{12} cm^{-3}$. At another density we would see differences in the cutoffs and the overall behavior of each mode, particularly at lower frequencies. Regardless of the density and

the mode we are considering, the dispersion relation approaches 1 as ω approaches infinity. As a result, picking a high frequency limits variations in the dispersion relation caused by changes in density, while also allowing us to treat the left and right-handed waves in the same manner that we would treat ordinary waves.

Using a high frequency is also advantageous from an optical standpoint. A beam with a higher frequency will be smaller, allowing the use of smaller optical components. A smaller beam at the receiver will result in a higher percentage of power being collected by our antenna. A narrow beam passing through the center of the chamber ensures that we are sampling a small chord of the plasma. Furthermore, increasing the frequency of our beam will lessen the effect of refraction caused by density gradients in the plasma. The interferometer, aimed at the center of the plasma, should be minimally affected as the direction of propagation is parallel to the refractive index gradients. On the other hand, the refractometer is aimed off center and is designed to measure these gradients. A higher frequency will keep the refracted beam in range of our detectors for a denser plasma.

The upper limit of our frequency is controlled by a number of concerns, few of which involve the actual plasma. One such concern is purely financial. The price for a 94 GHz Gunn oscillator is significantly lower than we would find at higher frequencies. Working at higher frequencies will not only increase the cost of the Gunn, but also the mixers, which need to be able to operate at the Gunn frequency.

Physically, vibrations caused by the polywell set the upper bound. At 94 GHz we are dealing with 3.19mm wavelengths. In this case it is unlikely that vibrations in the
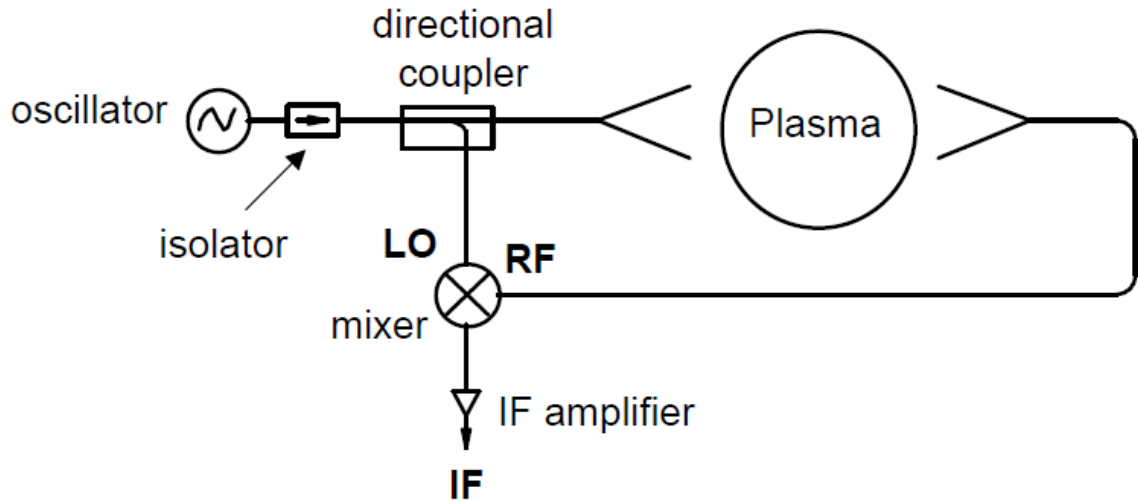
Figure 2-2. Basic schematic of a homodyne interferometer. "Excerpted from [*Gilmore*]"

machine will significantly alter the phase of our signal. For frequencies much higher, this

may become a serious concern.

This phase shift manifests itself primarily by altering the path length. The change

in the phase as a result of vibrations is equal to $2\pi l/\lambda$ where l is the change in path

length. Increasing the frequency will have a linear effect on the phase shift. This

problem is of particular concern for a low density plasma where the phase shift we are

measuring is small to begin with.

2.2 Homodyne interferometer

The basic design of a homodyne interferometer is shown in Figure 2-2. The term

homodyne refers to the fact that the same source is used by the mixer as both the received

signal and the local oscillator. A directional coupler splits the beam for its two uses,

typically sending most of the power into the plasma. Sending a powerful signal into the

plasma is necessary because power is lost as the beam propagates through the plasma,

and again at the receiver where the antenna collects only a fraction of the power

contained in the entire beam.

Once the signal has passed through the plasma it is mixed with the original split signal. The two signals entering the mixer can be defined by

$$V_{RF} = A_{RF}\cos(\omega t + \phi_{RF}) \qquad (2.5)$$

$$V_{LO} = A_{LO}\cos(\omega t + \phi_{LO}) \qquad (2.6)$$

where

V_{RF} is the voltage of the signal that passed through the plasma

A_{RF} is the amplitude of the RF signal

ω is the angular frequency of the Gunn

ϕ_{RF} is the phase offset of the RF signal

V_{LO} is the voltage of the local oscillator signal

A_{LO} is the amplitude of the LO signal

ϕ_{LO} is the phase offset of the LO signal

After passing through the mixer the new signal is

$$V_{IF} = V_{RF}V_{LO} = \frac{A_{RF}A_{LO}}{2}[\cos(2\omega t + \phi_{RF} + \phi_{LO}) + \cos(\phi_{RF} - \phi_{LO})] \quad (2.7)$$

which, ignoring the high frequency term, leads to

$$V_{IF} = \frac{A_{RF}A_{LO}}{2}\cos(\phi_{RF} - \phi_{LO}) = A_{IF}\cos(\Delta\phi) \qquad (2.8)$$

When there is no plasma present, or in the imaginary case of a constant plasma, $\Delta\phi$ will be constant and the output will be a DC value. Only when there is a change in the phase shift, caused by a growing or decaying plasma, will the interferometer have an oscillating output. A constant change in the plasma density would appear as a sinusoidal output with a fixed frequency. If the rate of change increased, the frequency of the sine wave would increase. The opposite would occur as the rate of change decreased.

2.3 Disadvantages of a Homodyne Interferometer

The most basic problem with the homodyne interferometer is that it is impossible to calibrate out amplitude variations created when a plasma is introduced. Equation 2.8 shows that the final signal depends on the phase shift as well as the amplitude of the two signals. As the RF signal passes through the plasma, power is lost to absorption and refraction. This will change the amplitude of the output signal and interfere with the extraction of the phase shift.

A subtler problem arises when trying to determine the direction of the phase shift. This problem occurs whenever the phase is 0, π, or 2π because cosine is an even function around these values. Any shift will lead to the same value regardless of direction. As a result, it is impossible to determine whether the phase has increased or decreased by π between these points. At times there can be information about the system which can clarify the direction; however this is not always the case.

The homodyne interferometer is a fairly simple circuit. With added complexity, we are able to eliminate these problems.

2.4 Heterodyne Interferometer

The design of the homodyne interferometer can be improved upon by using separate sources for the plasma and reference signals. This creates the heterodyne interferometer shown in Figure 2-3. The increased complexity makes it possible to distinguish between phase and amplitude changes.

The primary motivation behind adding a second source is that now the two signals entering the mixer can have different frequencies. Since both inputs have the same

frequency in the homodyne system, these frequencies cancel each other out in the low

frequency output term. When the frequencies are different, the output becomes:

$$V_{IF} = A_{IF} \cos\big((\omega_{RF} - \omega_{LO})t + \Delta\phi\big) \qquad (2.9)$$

where

ω_{RF} is the frequency of the RF Gunn

ω_{LO} is the frequency of the LO Gunn

This effect can be seen in Figure 2-4. For the homodyne interferometer, a phase

change moves the output frequency from zero. As a result, it is impossible to know the

direction of the frequency change. In the heterodyne interferometer, when the phase is

constant the output has frequency given by the difference between the two input

frequencies. The direction of a phase shift can now be seen as:

$$\Delta\omega = \Delta\omega^0 + \frac{d\phi}{dt} \qquad (2.10)$$

where

$\Delta\omega$ is the output frequency

$\Delta\omega^0$ is the difference between the two frequencies
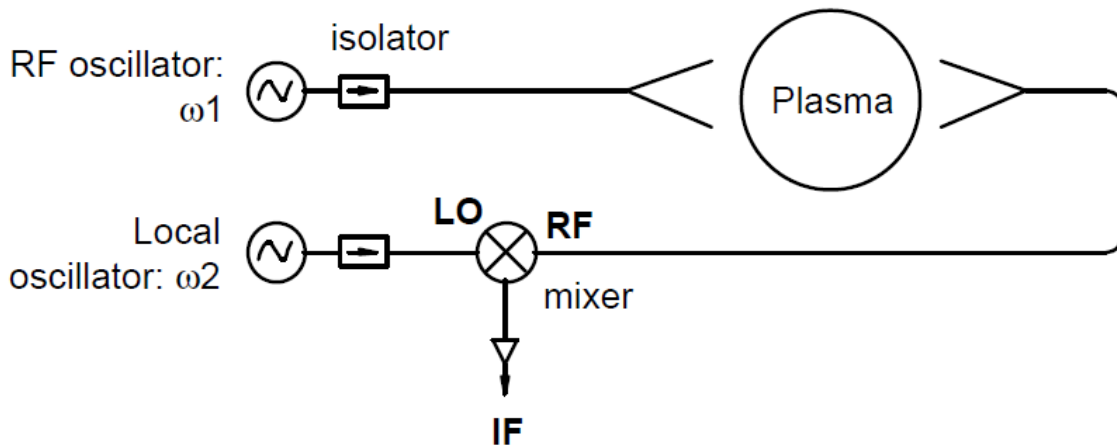
Figure 2-3. Heterodyne interferometer using two separate sources, "Excerpted from [*Gilmore*]"

12

$\frac{d\phi}{dt}$ is the phase shift

There are other advantages to a heterodyne

system that offset the added complexity and cost.

An obvious additional advantage to the heterodyne

system is that it will have more power available.

With the local oscillator signal powered by a

separate source, all of the power from the original

Gunn can be used for the beam that passes through

the plasma. The shift in the equilibrium output of

the mixers also eliminates the necessity of detecting

DC outputs.

Figure 2-4: Frequency shifts resulting from (above) homodyne and (below) heterodyne interferometers

Another method used to increase the accuracy

of an interferometer, while again adding complexity, is to include an I-Q mixer to provide

the final output signals.

2.5 I-Q Mixer

A primary concern when using a homodyne interferometer is the inability to

distinguish between a change in amplitude and a change in phase. An I-Q mixer can be

used to extract the phase change information by providing two output signals. One

output gives the same signal as a basic homodyne interferometer. The second output is

identical, except that it is 90 degrees out of phase.

The two outputs have signals given by

$$I = A\cos(\Delta\phi) \qquad\qquad (2.11)$$

$$Q = A\sin(\Delta\phi) \qquad\qquad (2.12)$$

13

In theory, the two signals will have identical amplitudes. By dividing one signal by the other, this amplitude can be eliminated, leaving a signal that varies only with phase change.

$$\frac{Q}{I} = \frac{A\sin(\Delta\phi)}{A\cos(\Delta\phi)} = \tan(\Delta\phi) \tag{2.13}$$

$$\Delta\phi = \tan^{-1}\left(\frac{Q}{I}\right) \tag{2.14}$$

In practice the amplitudes will not be identical, so the system must be calibrated to find the actual relationship. Once the system is calibrated, amplitude changes caused by the plasma should no longer affect the output. A decrease in the amplitude of the I channel with coincide with a proportional decrease in the amplitude of the Q channel.

2.6 Building an I-Q Mixer

It is possible to purchase an I-Q mixer that has already been built. In our case, the cost of an I-Q mixer that operated at the specific frequencies we are dealing with was too high. As a result we built a circuit that serves the same function.

Figure 2-5 shows the circuit that was built. We selected Gunn oscillators that were 500MHz apart. The first two mixers use the second Gunn, operating at 94.5GHz, as the local oscillator. One mixer has a direct path from the 94GHz RF Gunn as the other input, while the other uses the signal after it passes through the plasma. This gives us two signals

$$V_{IF}^{(1)} = A^{(1)}\cos\left((\omega_1 - \omega_2)t + \Delta\phi^{(1)}\right) \tag{2.15}$$

$$V_{IF}^{(2)} = A^{(2)}\cos\left((\omega_1 - \omega_2)t + \Delta\phi^{(2)}\right) \tag{2.16}$$

where

ω_1 is the frequency of the RF Gunn

14
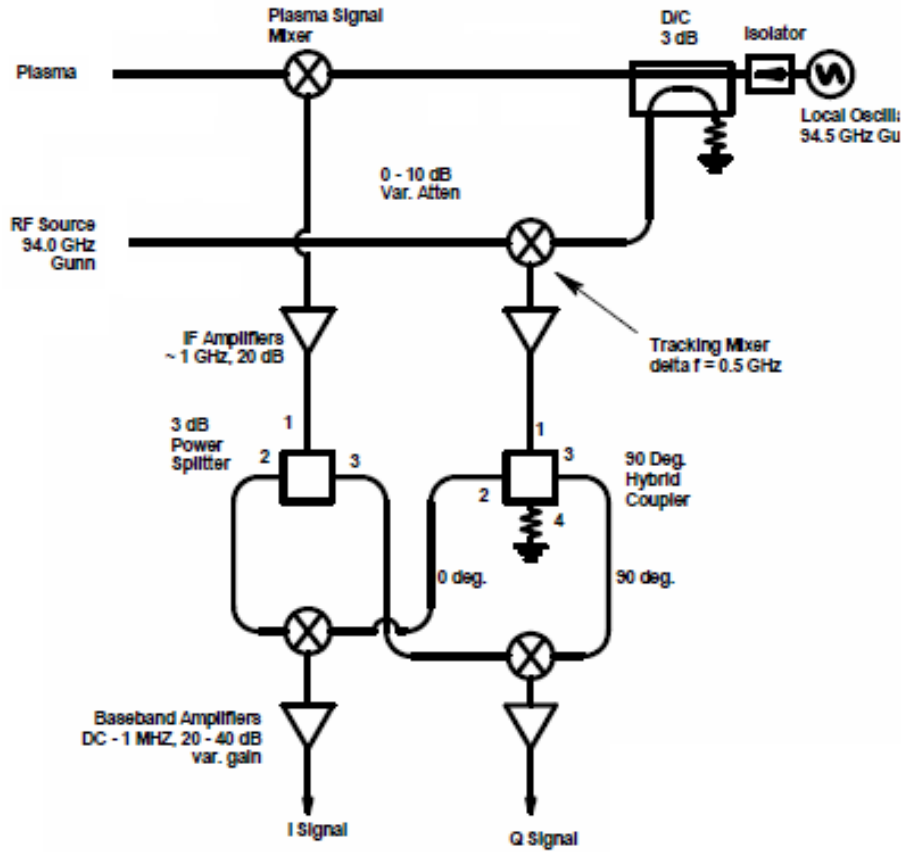
Figure 2-5: Schematic of the actual I-Q mixer that was built for our system

ω_2 is the frequency of the LO Gunn

and the signals have different amplitude and $\Delta\phi$ values. These outputs are put through

amplifiers and into power splitters. One of the power splitters has two identical outputs.

The other splitter has outputs that are 90 degrees out of phase. The two outputs of one

splitter are each mixed with one of the outputs of the other splitter. The resulting signals

are

$$I = \frac{A^{(1)}A^{(2)}}{2}\left[\cos\left(2\omega_0 t + \Delta\phi^{(1)} + \Delta\phi^{(2)}\right) + \cos\left(\Delta\phi^{(1)} - \Delta\phi^{(2)}\right)\right] \quad (2.17)$$

$$Q = \frac{A^{(1)}A^{(2)}}{2}\left[\cos\left(2\omega_0 t + \Delta\phi^{(1)} + \Delta\phi^{(2)} + \frac{\pi}{2}\right) + \cos\left(\Delta\phi^{(1)} - \Delta\phi^{(2)} - \frac{\pi}{2}\right)\right] \quad (2.18)$$

15

where ω_0 is $(\omega_1 - \omega_2)$

There is an additional complication now that there are two different phase shifts to consider. This additional phase shift can be calibrated out by finding $\Delta\phi^{(1)}$, resulting from the reference leg of the system, which should not change. These signals are put through amplifiers that pass the lower frequency portion of the signal yielding

$$I = A\cos\left(\Delta\phi^{(2)} + C\right) \tag{2.19}$$

$$Q = A\cos\left(\Delta\phi^{(2)} + C + \frac{\pi}{2}\right) \tag{2.20}$$

where

A is $\frac{A^{(1)}A^{(2)}}{2}$

C is the constant found from calibrating $\Delta\phi^{(1)}$

2.7 Actual Interferometer Circuit

Figure 2-6 shows the interferometer circuit that was built. We used a heterodyne system with an RF Gunn oscillator that operated at 94 GHz. The local oscillator Gunn runs at 94.5 GHz. This yields a ω_0 value of 500 MHz. Attenuators were placed between the Gunns and the LO input of the mixers to keep the power between 10 and 13 dBm. Before measuring the signal, the outputs from our I-Q mixer are put through amplifiers with variable gains between 60 and 80 dBm.

2.8 Calculating the Plasma Density

The geometry of the entire system is important to consider, particularly the relationship between the direction of propagation and the magnetic field. In the case of our plasma, the direction of propagation for our wave is parallel to the magnetic field in
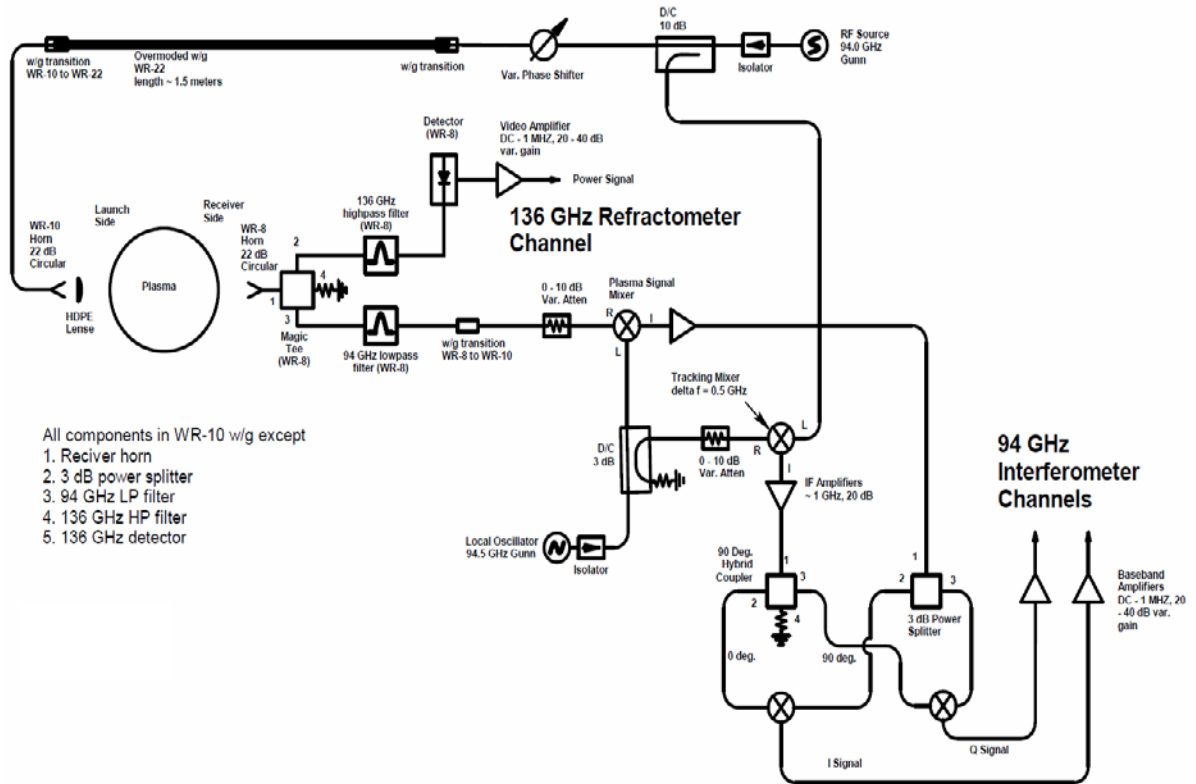
Figure 2-6: Schematic for our 94 GHz interferometer. Also included is the 136 GHz refractometer

the plasma. As a result, there are two kinds of waves that will propagate; left-hand waves and right-hand waves. As discussed previously, by using a high enough frequency these waves can be treated as ordinary waves.

The effect the plasma density has on the total phase shift of the signal is given by

$$\phi = \int kdl = \int n_0 \frac{\omega}{c} dl \qquad (2.21)$$

where

ϕ is the total phase lag

ω is the frequency of the beam

k is the wave number

c is the speed of light in free space [*Hutchinson*]

and n_0 is the refractive index of the plasma in O-mode, defined as

17

$$n_0{}^2 = 1 - \frac{\omega_p^2}{\omega^2} = 1 - \frac{n_e}{n_c} \tag{2.22}$$

where

n_e is the time varying electron plasma density

and n_c is the cutoff density where the O-mode waves will no longer propagate. One of

the reasons why it is easier to consider O-mode waves is that they do not depend on the

magnetic field. The cutoff density is

$$n_c = \frac{\omega^2 m_e \epsilon_0}{e^2} \tag{2.23}$$

Where

m_e is the mass of an electron

ϵ_0 is the permittivity in free space

e is the charge of an electron

   The equation for the phase lag has a single value that varies with position in the

plasma and that is n_e. Since we cannot measure each point separately we can replace this

term with a constant n_{avg} and solve for the line average density. In this case, after

pulling everything out of the integral the equation becomes

$$\phi = \frac{\omega}{c} \sqrt{1 - \frac{n_{avg}}{n_c}} \int dl = \frac{\omega l}{c} \sqrt{1 - \frac{n_{avg}}{n_c}} \tag{2.24}$$

where l is the path length through the plasma. [*Hutchinson*]

   This allows us to compare the density to the total phase lag, but the output of our

interferometer gives us the phase change over time. We can change ϕ to $\Delta\phi$ by writing

the equation instead as

18

$$\phi = \int \left(k_{plasma} - k_0 \right) dl \qquad (2.25)$$

where

k_{plasma} is the wave number with a plasma present

k_0 is the wave number without a plasma

Without a plasma the wave number $k_0 = \omega/c$ so equation 2.24 becomes

$$\Delta\phi = \frac{\omega l}{c} \left[\sqrt{1 - \frac{n_{avg}}{n_c}} - 1 \right] \qquad (2.26)$$

which can be solved for

$$n_{avg} = n_c \left(1 - \left(1 + \frac{c\Delta\phi}{\omega l} \right)^2 \right) \qquad (2.27)$$

[*Hutchinson*]

This yields the line average density which is the best that can be done using the

interferometer.

2.9 O-mode Assumption

Now that we have a formula for finding the density of a plasma based on the

assumption that waves are in O-mode, it is important to verify that this is a reasonable

approximation for the R and L modes that are actually propagating. The simple formula

for n_c in equation 2.23 holds true for O-mode waves. The cutoff for R and L waves are

more complicated, given by

$$n_c = \frac{\epsilon_0 \omega}{e^2} \left[\frac{m_i m_e (\omega + \omega_{ci})(\omega - \omega_{ce})}{m_i(\omega - \omega_{ce}) + m_e(\omega + \omega_{ci})} \right] \qquad (2.28)$$

$$n_c = \frac{\epsilon_0 \omega}{e^2} \left[\frac{m_i m_e (\omega - \omega_{ci})(\omega + \omega_{ce})}{m_i (\omega + \omega_{ce}) + m_e (\omega - \omega_{ci})} \right] \qquad (2.29)$$

where m_i is the mass of the ions

for R and L mode, respectively. For our particular system the frequency is 94GHz,

deuterium is the ion species, the plasma is assumed to be 18cm in diameter, and a

magnetic field strength of .17 T is approximately what the beam will encounter as it

passes through the plane of a coil.

Using these values, along with equation 2.27, we can find the density that

corresponds to a 2π phase shift for each kind of wave. In each case a 2π phase shift

indicates a density of $3.93*10^{18}$ m^{-3}. The difference between the O-mode density and the

R or L mode densities is on the order of 10^{15}. This is why high frequency was selected.

As $\omega \to \infty$ the part of 2.28 and 2.29 in brackets approaches ω. So as the frequency

increases, the R and L mode cutoff densities approach 2.23, the O-mode cutoff.

3.1 Gaussian Beam Propagation

It would be extremely difficult to solve the full wave equation for our system. We would need to describe an electromagnetic wave that is transmitted by a corrugated horn antenna before passing through a lens, two ports of a chamber and a plasma. Fortunately the beam exiting our antenna can be well approximated as a Gaussian beam. In Gaussian optics the wave equation is simplified using the paraxial approximation, which assumes a wave that is relatively collimated. The approximation holds true provided that the angle of divergence is less than ~30 degrees from the direction of propagation. When our beam leaves the antenna it has a divergence angle of ~ 19 degrees. It is even smaller once the beam interacts with the lens. Another criterion for using Gaussian optics is that all optical components must be large compared to the wavelength. This can lead to some challenges when building the physical system.

The intensity of the beam has a Gaussian distribution as we move radially outward from the center. We define the spot size of the beam as the distance from the beam's center at which the intensity drops to e^{-2} of the peak intensity. Displaying the spot size of a beam as it propagates, therefore, will only account for 86.5% of the power contained in the entire beam.

For a specific wavelength the complex beam parameter is used to fully describe a beam at each point as it propagates. The real term, z, tells how far a point is from the beam waist. The imaginary term, z_R, is the Rayleigh length which is the distance from the beam waist to the point where the beam area doubles. This term contains the information about the angle of divergence and the spots size at the beam's waist.
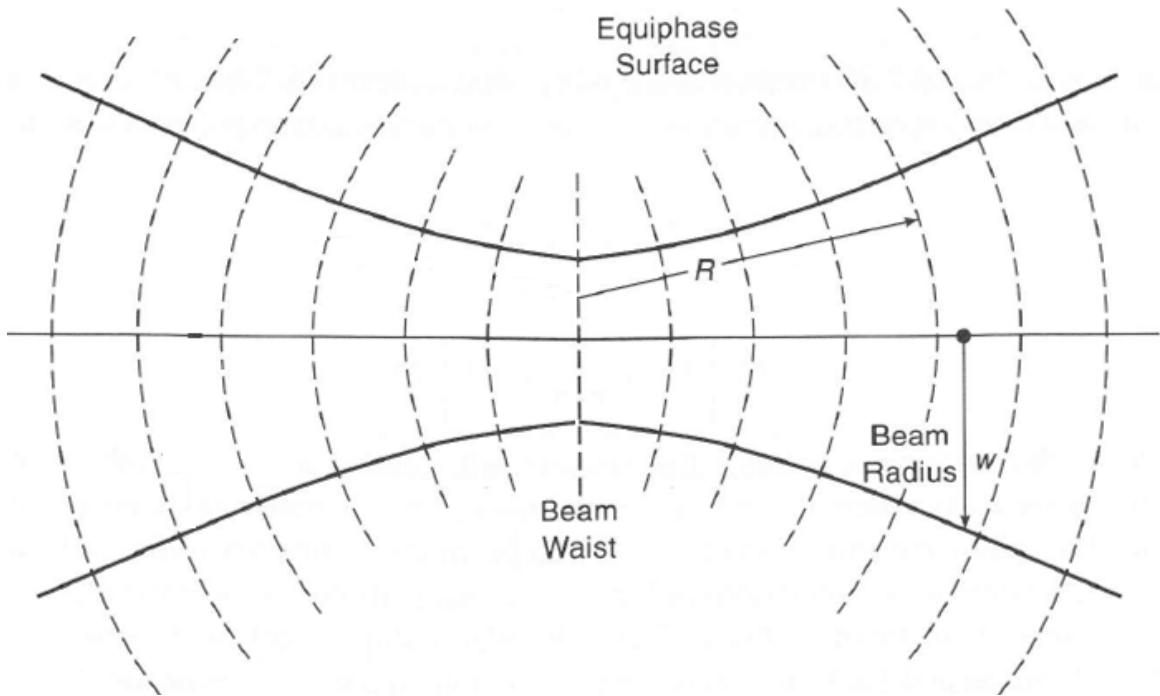
Figure 3-1: Gaussian beam propagating from left to right.

$$z_R = \frac{\pi \omega_0^2}{\lambda} \qquad (3.1)$$

where:

ω_0 is the beam waist

λ is the wavelength.

Figure 3-1 plots the spots size of a Gaussian beam as it propagates from left to right. The imaginary part of the complex beam parameter defines the shape of the entire beam. The real part simply tells us where the beam waist is located. When the real part is negative, it indicates that the beam is focusing and tells us how far the beam must travel before it is fully focused. A positive real part indicates that the beam is expanding and the magnitude reflects how far the beam has traveled past its waist.

3.2 Corrugated Horn Antenna

TABLE 7.1 Parameters[1] for Optimum Coupling of Various Feed Structures to Fundamental Mode Gaussian Beam

Feed type	w/a	$\|c_0\|^2$	ϵ_{pol}	$\epsilon_{pol}\|c_0\|^2$
Corrugated circular	0.64	0.98	1.0	0.98
Corrugated square	0.35	0.98	1.0	0.98
Smooth-walled circular[2]	0.76	0.91	0.96	0.87
Smooth-walled circular[3]	0.88, 0.64	0.93	0.96	0.89
Dual-mode	0.59	0.98	0.99	0.97
Rectangular[4]	0.35, 0.50	0.88	1.0	0.88
Rectangular[5]	0.35	0.88	1.0	0.88
Square[6]	0.43	0.84	1.0	0.84
Rectangular[7]	0.30	0.85	1.0	0.85
Diagonal	0.43	0.93	0.91	0.84
Hard	0.89	0.82	1.0	0.82
Corner cube	$1.24\,\lambda$	—	—	0.78
Hybrid mode	0.64	0.98	1.0	0.98
Slotline	—	—	—	0.80
Lens + planar antenna[8]	—	—	—	0.89

Table 3-1: Parameters for optimum coupling for different feed horn geometries [*Goldsmith*]

Most horn antennas have a small enough divergence angle such that the paraxial approximation holds. We selected our particular antenna to maximize the correlation between the transmitted signal and an ideal Gaussian beam. Table 3-1 shows how well the signal transmitted by horns with different geometries can be coupled to a Gaussian beam. The $\|c_0\|^2$ column indicates how strongly the beam couples to a true Gaussian beam while the w/a column indicates the spot size of the beam depending on the size of the aperture. Ideally we aren't concerned with the polarization of the beam, indicated by ϵ_{pol}, though as we will discuss later, this could play a role in the real system. The best coupling occurs when a corrugated horn is used.
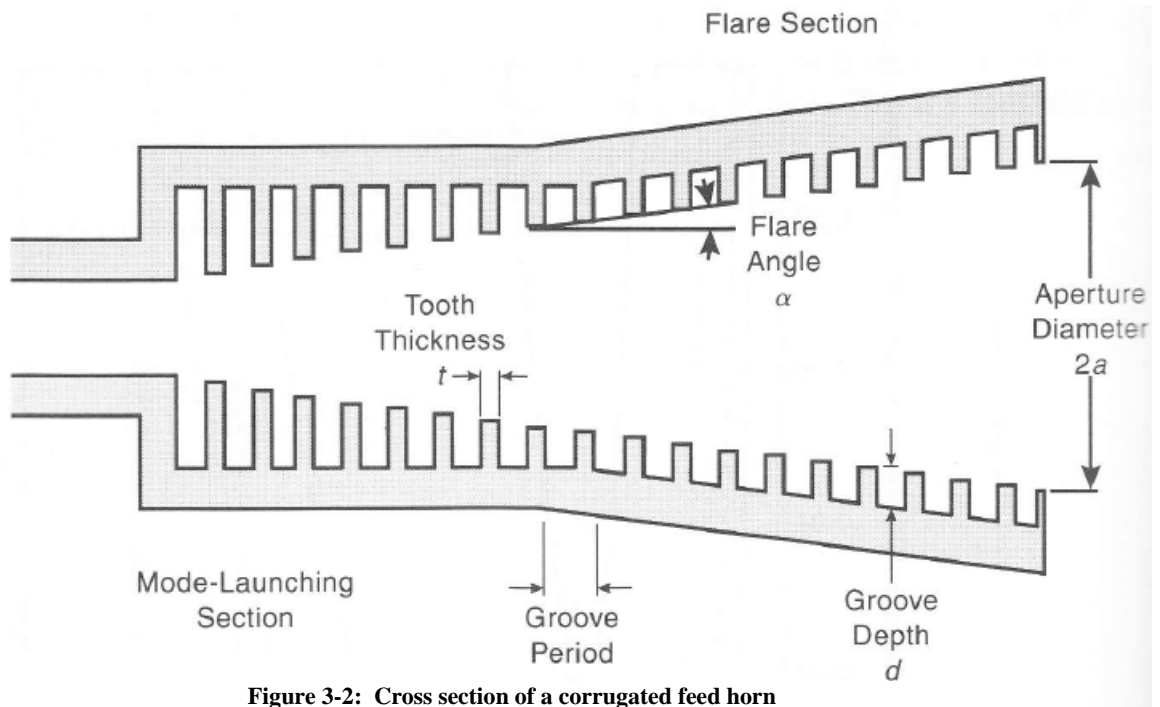
Figure 3-2: Cross section of a corrugated feed horn

The improved coupling in corrugated horns is a result of the reactance created by the grooves. Figure 3-2 shows the cross section of a corrugated feed horn. The reactance caused by the grooves related to the impedance of free space by

$$\frac{X_s}{Z_0} = \tan\left(\frac{2\pi d}{\lambda}\right) \qquad (3.2)$$

where

d is the depth of the grooves

X_s is the reactance

Z_0 is the impedance of free space

When the depth of the grooves is a quarter of the signal's wavelength the reactance is infinite. This is referred to as the balance hybrid condition and results in the strongest correlation between the transmitted wave and a true Gaussian beam. The relationship between the groove depth and the wavelength means that a particular corrugated horn will only work well for a small range of frequencies. This relationship

24
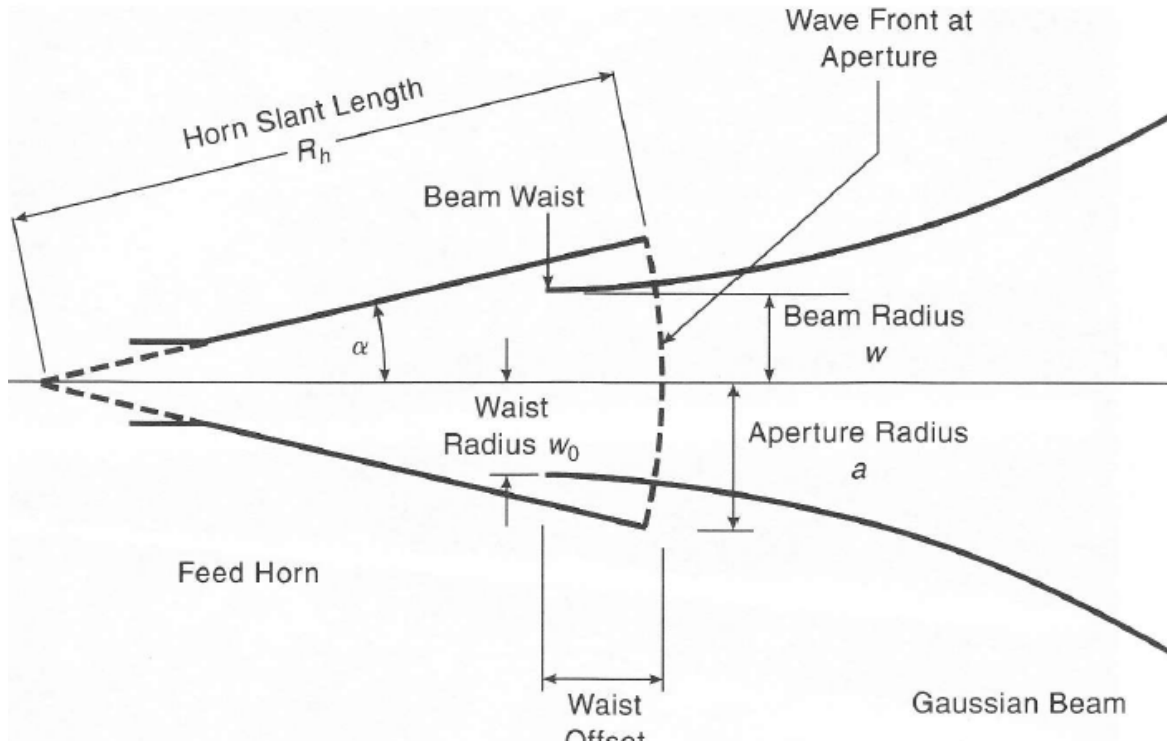
Figure 3-3: Cross section of the Gaussian beam transmitted by a feed horn

also exists for the spacing of the grooves, which must be significantly less than a wavelength. It is important to note that the grooves farthest from the aperture are deeper than the rest. This transition from deep grooves to the quarter wavelength grooves ensures that the wave transmitted operates in the principle HE_{11} mode, converted from the TE_{11} mode propagating in the waveguide.

As we have seen, in order to define the Gaussian beam produced by a feed horn we need to find the position and size of the beam waist. Locating the waist of a Gaussian beam can be done a number of ways, one of which is to find the beam's radius of curvature. The radius of curvature is the shape of the wave front at which the signal has a constant phase. For the beam exiting a feed horn, the radius of curvature is equivalent to the horn's slant length. Figure 3-3 shows the beam transmitted by a feed horn. While the

horn will not physically come to a point as shown, the horn slant length can be solved for

using:

$$R_h = \frac{a}{\sin \alpha} \qquad (3.3)$$

where

R_h is the slant length

a is the aperture radius

α is the flare angle

     The spot size leaving the antenna depends on the type of horn we are using. The

previously referenced Table 1 not only shows how strong the coupling is for a particular

geometry, it also tells us how the spot size leaving the lens corresponds to the aperture

radius. For a corrugated circular horn the relationship is w/a = .644.

     Once we have the radius of curvature and the spot size leaving the lens, the

following equations can be used to find the spot size and location of the waist

$$\omega_0 = \frac{\omega}{\sqrt{1 + \left(\pi\omega^2 / \lambda R \right)^2}} \qquad (3.4)$$

$$z = \frac{R}{1 + \left(\lambda R / \pi\omega^2 \right)^2} \qquad (3.5)$$

Using ω_0 to solve for z_R gives us the complex beam parameter for the Gaussian beam

which best approximates the wave transmitted by the feed horn.

3.3 Ray Transfer Matrix

One of the benefits of defining a Gaussian beam using its complex beam parameter is that it allows us to easily calculate the beam that is created when the beam propagates through different quasi-optical components. The formula for calculating a new beam is:

$$\begin{pmatrix} q_2 \\ 1 \end{pmatrix} = k \begin{pmatrix} A & B \\ C & D \end{pmatrix} \begin{pmatrix} q_1 \\ 1 \end{pmatrix} \qquad (3.6)$$

where

q_1 is the original complex beam parameter

q_2 is the new complex beam parameter

k normalizes the second term to 1

and the ABCD matrix defines the path that the beam has taken.

The path of our beam can be divided into two distinct situations. The first is a beam traveling a distance L through any uniform medium. The corresponding ABCD matrix is given by:

$$\begin{pmatrix} 1 & L \\ 0 & 1 \end{pmatrix} \qquad (3.7)$$

When a beam is propagating through a uniform medium it is not necessary to use the ray transfer matrix. The real part of the beam tells us how far we are from the waist, so propagating a distance L simply requires us to add L to the complex beam parameter, leaving the imaginary part unchanged. The value of having an ABCD matrix for this scenario arises when the beam passes into new mediums and the entire path needs to be combined into a single matrix.

The second situation occurs when a beam passes through a curved interface. The ABCD matrix is:

$$\begin{pmatrix} 1 & 0 \\ \dfrac{n_2 - n_1}{n_2 R} & \dfrac{n_1}{n_2} \end{pmatrix} \tag{3.8}$$

where n_1 and n_2 are the refractive indexes of the first and second materials, respectively, and R is the radius of curvature. $R > 0$ corresponds to a surface that is concave to the left for a beam propagating right. For a flat surface, we take $R \to \infty$. When a beam passes through any interface between two different mediums with different indexes of refraction both the real and imaginary terms in the complex beam parameter will be altered.

Any path of propagation can be defined by a single ABCD matrix. In order to find this matrix, the separate matrices of each interface and each length of propagation through constant media are multiplied together in the reverse order in which the wave encounters them. The system we are designing involves propagation through free space to the first curved interface of the lens, followed by propagation through the lens material to the flat interface of the lens, and finally, propagation through free space to the receiving end of the chamber. The resulting ABCD matrix for the beam leaving our lens looks like:

$$\begin{pmatrix} 1 & 0 \\ 0 & \dfrac{n_2}{n_1} \end{pmatrix} \cdot \begin{pmatrix} 1 & L \\ 0 & 1 \end{pmatrix} \cdot \begin{pmatrix} 1 & 0 \\ \dfrac{n_2 - n_1}{n_2 R} & \dfrac{n_1}{n_2} \end{pmatrix}$$

$$\Rightarrow \begin{pmatrix} 1 + \dfrac{(n_2 - n_1)L}{n_2 R} & \dfrac{n_1 L}{n_2} \\ \dfrac{n_2 - n_1}{n_1 R} & 1 \end{pmatrix} \tag{3.9}$$

Solving for the real and imaginary parts of the new complex beam parameter can be done using:

$$Re[q_2] = \frac{(Re[q_1])^2 AC + Re[q_1]AD + (Im[q_1])^2 AC + Re[q_1]CB + BD}{(Re[q_1]C)^2 + 2Re[q_1]CD + D^2 + (Im[q_1]C)^2} \qquad (3.10)$$

$$Im[q_2] = \frac{Im[q_1](AD - BC)}{(Re[q_1]C)^2 + 2Re[q_1]CD + D^2 + (Im[q_1]C)^2} \qquad (3.11)$$

When the final system is used as an interferometer the beam will also pass

through a plasma. Unfortunately we know very little about the plasma that we will be

dealing with so it is impossible to say what affect it will have on the shape of our beam.

The hope is that the beam encounters a plasma that is relatively symmetrical about the

center of the chamber, so that each effective interface that the beam encounters as it

propagates toward the center of the plasma will correspond to a similar, but reversed,

interface as it propagates out of the plasma. For our interferometer we expect this

approximation to be sufficient. When we begin to examine the beam in our refractometer

the exact density profile of the plasma will be of vital importance.

3.4 Desired Gaussian Beam

The goal of this experiment is to propagate a Gaussian beam through the center of

a plasma, receive the signal and determine the phase shift. The ideal wave would be a

very narrow, collimated beam. A narrow beam entering the chamber would allow us to

use smaller optical components and transmit multiple beams into the chamber

simultaneously. A narrow beam passing through the plasma will assure us that we are

sampling a thin chord and our results are not being affected by the entire plasma. It may

be most important to have a narrow beam at the receiver. A smaller spot size as the beam

exits the chamber will result in a higher percentage of the beam's power passing through

the aperture of our receiver antenna.

Unfortunately, the waist size of a Gaussian beam is inversely proportional to its

angle of divergence by:

$$\theta \cong \frac{\lambda}{\pi \omega_0} \hspace{3cm} (3.12)$$

As a result, the more collimated our beam is, the larger the waist. Figure 3-4 shows how

this looks for three different beam waists. The chamber is ~2 meters wide and our

vacuum wavelength is 3.1915mm. In each case the waist is located at the center of the

chamber. It is easy to see that creating a narrow beam in the plasma itself will increase

the size of our front-end optics and decrease the power received. This is what dictates

our physical limits. We need to have enough power received to interpret the signal, and

we only have a 12-inch window to launch the beam through.

3.5 Diffraction Limit

Sending a Gaussian beam through any aperture will result in some beam

truncation. The spot size of a beam is drawn as a solid line showing the shape of the

beam, but that line represents a portion of the beam which only contains 86.5% of the

total power. In order to avoid large diffraction effects, it is best to use optical

components that have a diameter at least four times the spot size of the Gaussian beam

passing through it [*Goldsmith*].

A more rigorous method of dealing with beam truncation can be done which finds

a different Gaussian beam created by the aperture. It is far from a perfect system, as it

ignores the effect of the truncation on side lobes, instead focusing on how the main lobe

is broadened by the aperture. The relationship between the original beam and the new

effective beam for moderate levels of truncation, $\leq 20dB$, is found using:
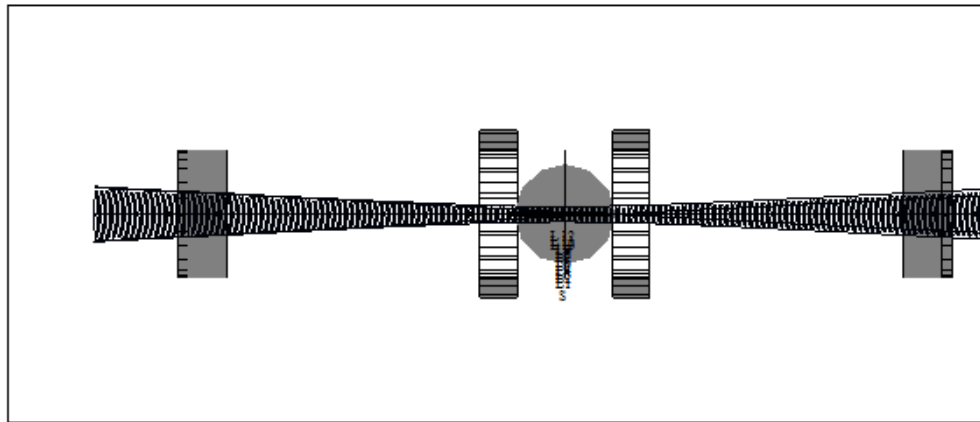
94GHz, 1.8cm waist
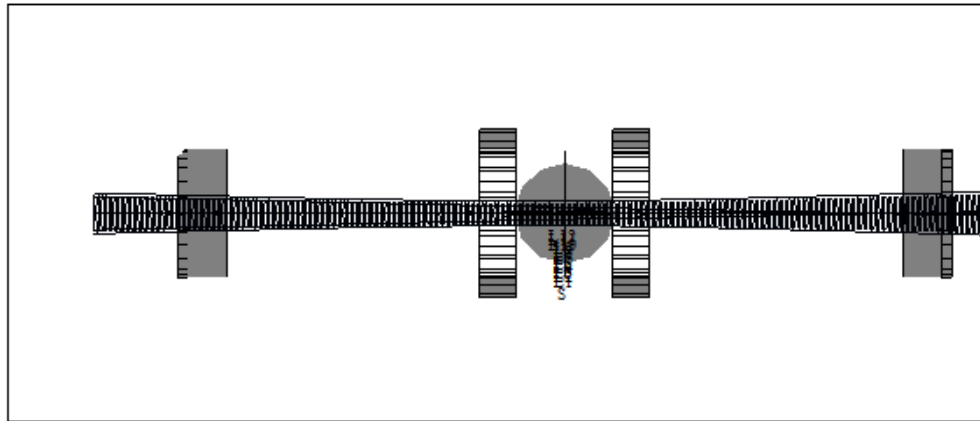
94GHz, 2.9cm waist
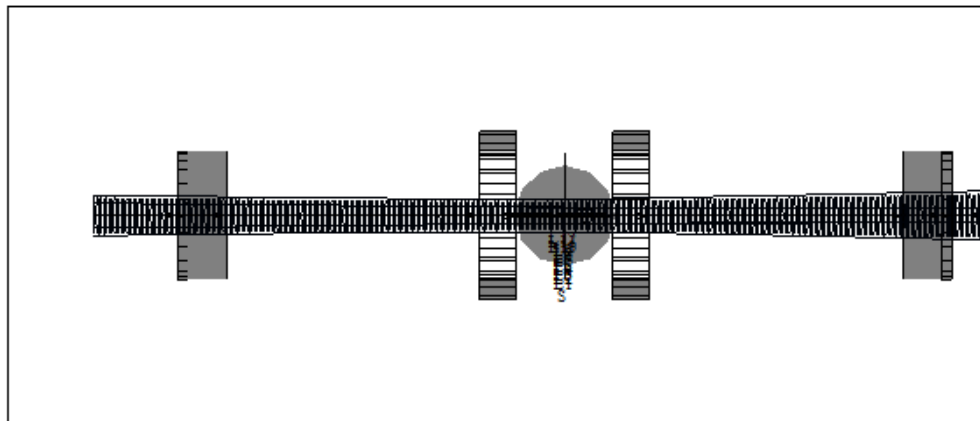
94GHz, 3.9cm waist

Figure 3-4: Gaussian beams with different waist sizes located in the center of the chamber

$$\frac{\omega_{0eff}}{\omega_0} = \frac{0.40\sqrt{T_e(dB)}}{1.6 + 0.021T_e(dB)} \qquad (3.13)$$

where

ω_{0eff} is the new effective beam waist

ω_0 is the original beam waist

Te (dB) is power lost due to the beam truncation.

This results in two separate problems. In addition to simply losing power as the beam passes through an aperture, the effective waist of the new beam is smaller. A smaller waist means that our beam will have a larger angle of divergence. Since we want our beam to be as collimated as possible, it is this result that prevents us from simply using lenses with a smaller diameter.

3.6 Beam Waist Position

The limitation placed on the size of our front end optics comes from space constraints on the physical system. We intend to aim the interferometer channel through the center of a 12-inch diameter window. Also sending signals into the chamber is a refractometer channel. While the operation of the refractometer is quite a bit different, the front-end optics are almost identical. Eventually, the hope is to add a second refractometer channel. Figure 3-5 shows this desired geometry. Not only are the refractometers supposed to fit next to the interferometer, but they are also supposed to have range of motion. We want it to be able to move parallel to the port window along one dimension so that we can take measurements through different chords. In order to have space for multiple lenses, and space left over for range of motion, these lenses needed to be kept as small as possible.
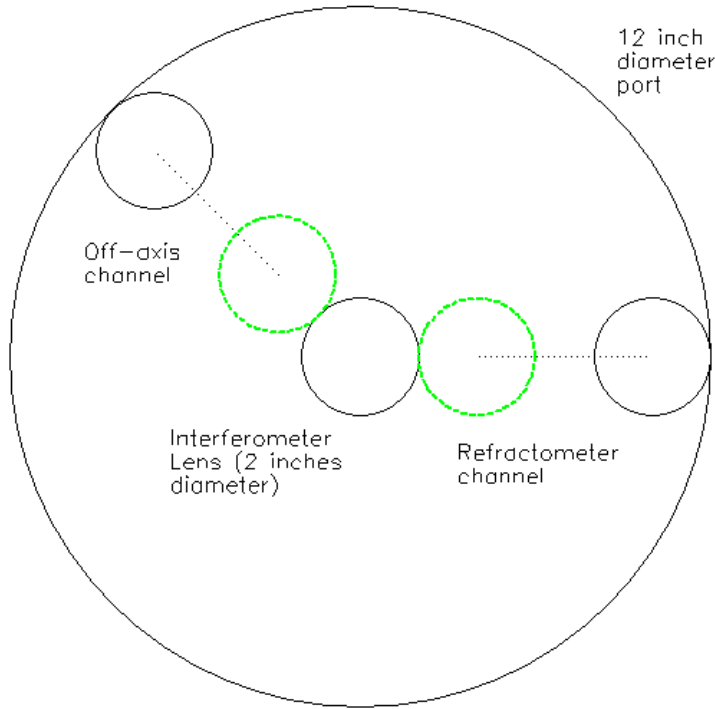
Figure 3-5: Layout of front-end optics using 2 inch lenses

This leads to a new challenge. Once we set a maximum spot size for our beam as it leaves the lens, we have fully specified a set of possible beams that can be transmitted. If this spot size is not large enough, the set may not contain a beam with a waist in the center of the chamber. To see this limit, a Mathematica script was written to find the maximum distance from the waist a signal could be when it has a given spot size. I used the equation

$$z = \pm \frac{\pi \omega_0^2}{\lambda} \sqrt{\left(\frac{\omega}{\omega_0}\right)^2 - 1} \qquad (3.14)$$

where

z is the distance from the waist

ω_0 is the spot size at the waist

λ is the wavelength of the beam

ω is the spot size leaving the lens

Even if we know the spot size leaving the lens the beam can take on many different shapes, defined by the beam's waist. The largest possible waist size is the spot

33

size of the beam leaving the lens. The smallest spot size approaches zero. My code finds the waist size in this range that will be located as far as possible from the lens. The results are plotted in Figure 3-6.

The first thing to notice is that we need a fairly large beam to put the waist in the center of the chamber, 1 meter away. In fact, it isn't even until the spot size is nearly 5 cm that we can put the waist where we want it to be. As previously mentioned, the diameter of any optical component needs to be at least 4 times the spot size before we can even think about ignoring diffraction. Unfortunately, this would require us to use lenses that are 20 cm in diameter. Two lenses of this size couldn't fit side by side in the window, and we certainly couldn't have one centered in the window and use the other in any way.

When the decision was made to use optics smaller than this, another issue was raised. While having the waist in the center of the chamber was our best-case
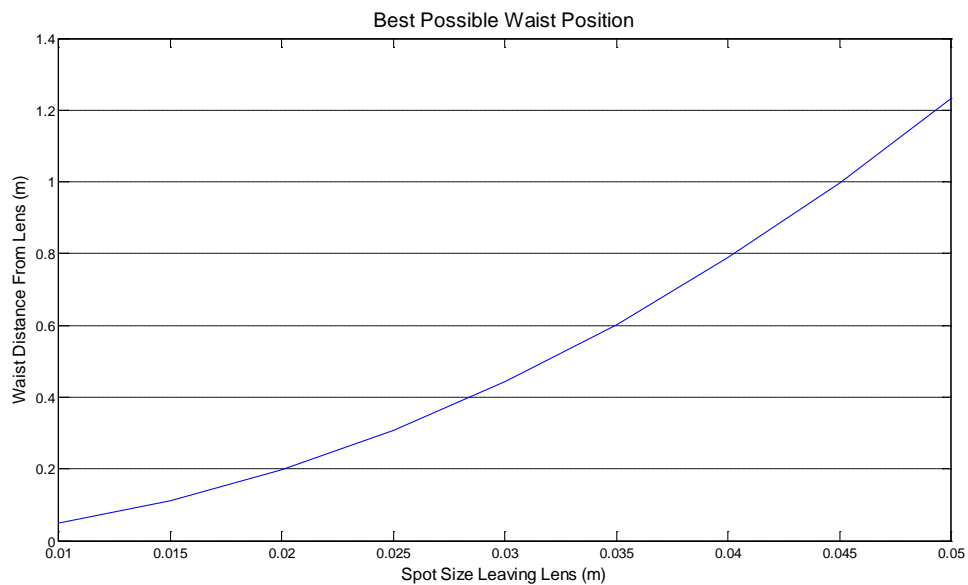
Figure 3-6: Farthest possible position of the beam waist for a given spot size
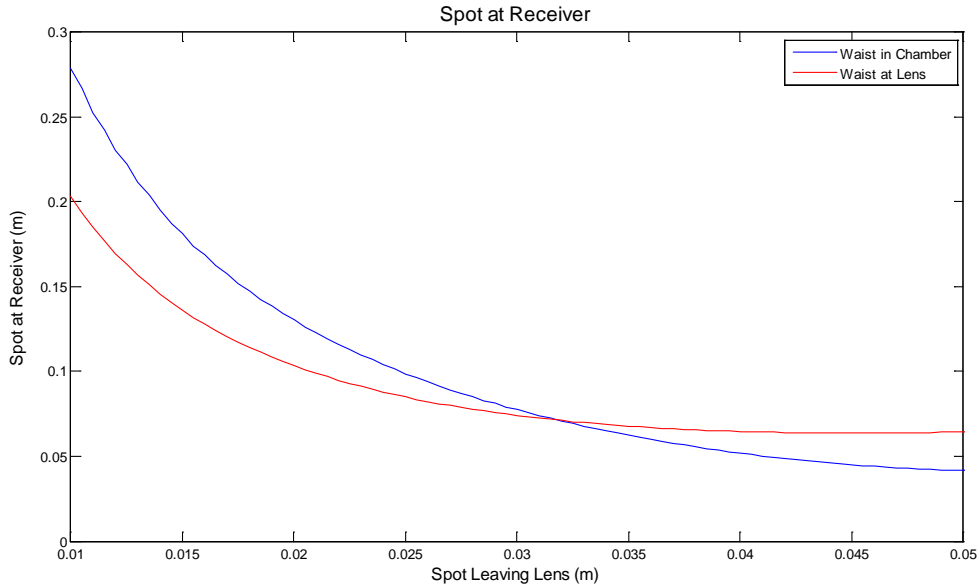
Figure 3-7: Spot size at the receiver for different waist locations

scenario, if this is not possible we don't necessarily want the waist as far into the

chamber as possible. The reason for this is the inverse correlation between the waist size

and the angle of divergence that we saw in a previous section. This can be seen clearly in

Figure 3-7.

The blue plot represents the spot size at the receiver that results when the waist is

as far from the lens as possible. The red plot shows the spot size at the receiver when the

waist is located at the lens. When we can put the waist close to the center it is best to do

so. On the other hand, when we can only put the waist half a meter into the chamber or

less, it is actually to our advantage for the waist to be larger and located at the lens.

There is an additional advantage to a beam with its waist located at the lens. As

the beam passes through the plasma, we would like the beam to be as collimated as

possible. If the beam has a narrow waist located just before encountering the plasma, it

will expand quickly and the portion of the beam measured by our receiver will represent

a chord that is quite a bit larger as it passes through the second half of the plasma. There

35

are only two ways that we can create a more collimated beam. The first is to increase the frequency. Since this wasn't an option, the only other way in to increase the waist size. The largest possible waist size is created when the waist is located at the lens.

3.7 Received Power

There are two characteristics we want to see from our beam at the receiver. The first is that we would like the spots size to be the same as it was entering the chamber. This would tell us that we have put the beam waist at the center of the plasma. If we aren't able to achieve this, then we want as small a beam as possible. A smaller spot size will lead to more power received in the small fixed aperture at the entrance to our receiving horn antenna.

Calculating the percent of the total power passing through an aperture is made easier by our selection of a circular receiving horn. When a Gaussian beam passes through a round aperture, the power that is transmitted is given by

$$P = P_0 \left[1 - e^{-2r^2/\omega^2} \right] \qquad (3.15)$$

where

P_0 is the total power in the beam

r is the radius of the aperture

ω is the spot size of the beam

Figure 3-8 shows how the spot size affects the power received for the antenna we are using. The radius of our receiving horn is .653 cm. Having such a small aperture allows us to take a more accurate measurement. The portion of the beam collected by our antenna should have passed through a very narrow portion of the plasma. As we can see

Percent of Power Received
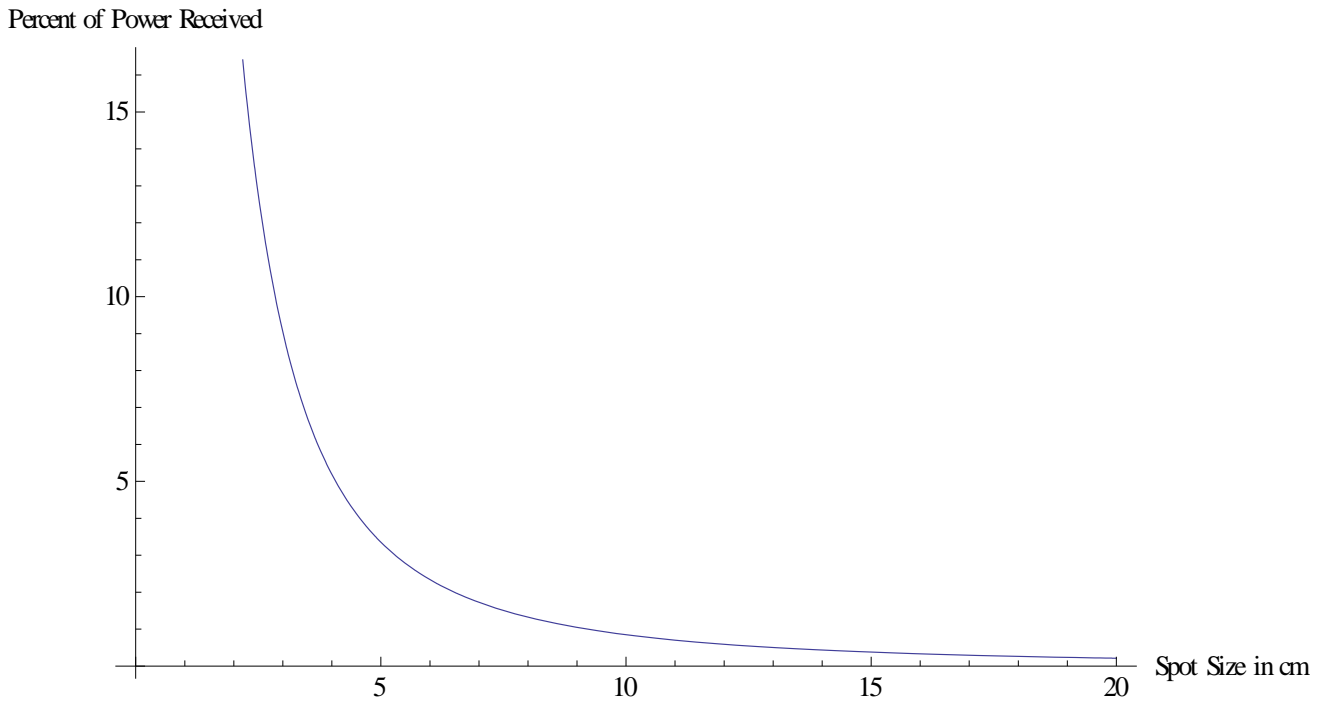
Figure 3-8: Power received for different spot sizes at the receiver

from the figure, we are expecting to detect only a small portion of the entire beam.

Additional power will be lost by absorption and refraction in the plasma.

To make sure we are able to receive a signal that can be carefully measured, we

need to use Gunn oscillators that can create a powerful beam. The signal leaving our

Gunn has a power measured at 17 dBm. This power is split into two beams, one that is

sent through the plasma and the other that is simply a reference. Because of the power

need by the transmitted beam, the power is split using a 10 dB directional coupler. As a

result, the power in the transmitted beam is still around 16.5 dBm.

3.8 Lens Selection

Much of what was considered in the previous sections could not be implemented

on this experiment due to space limitations. As a result, we designed a lens that would

put the waist in the middle of the chamber, but was only 14 cm in diameter. The

complexities created by the introduction of diffraction increased the importance of bench

tests to find the actual behavior of the optics.

In order to create a lens, first we need to know the beam we want to exit the lens.

In our case we wanted a beam that was 1 meter from the waist and with the smallest

possible spot size leaving the lens. From Figure 3-6 we can see in order to put the waist

in the center of the chamber the spot size leaving the lens cannot be smaller than ~4.8cm.

When we solve for the corresponding beam waist, it is approximately 3cm. This results

in a complex beam parameter of

$$z = -1 + .885929i \qquad (3.16)$$

where the negative real term indicates that the beam leaving the lens is focusing.

Once we know the beam we want leaving the lens we can begin working

backward. The next easy step is to find the beam just before it leaves the lens. The side

of the lens facing our chamber is flat. The ABCD matrix for a beam passing through a

flat interface is

$$\begin{pmatrix} 1 & 0 \\ 0 & \dfrac{n_1}{n_2} \end{pmatrix} \qquad (3.17)$$

where

n_1 is the refractive index of the first material, in this case high density polyethylene

(HDPE = 1.5187)

n_2 is the refractive index of the second material, in this case free space (1.0)

Solving for the beam in the lens gives us

$$z = -1.5187 + 1.3455i \qquad (3.18)$$

Now we need to consider the beam leaving the antenna. The beam in the lens is a

constant value that we are trying to create. There are a number of variables that we can

38

change. The first obvious one is the curvature of the lens. The other two variables both relate to how the complex beam parameter changes as it propagates through a constant medium. The ABCD matrix is

$$\begin{pmatrix} 1 & L \\ 0 & 1 \end{pmatrix} \tag{3.19}$$

where L is the distance traveled. The new complex beam parameter will have the same imaginary term, but will have L added to the imaginary term.

Propagation in a constant medium occurs in two parts of our system. First, the beam leaving the antenna travels through free space until it hits the curved portion of the lens. We can alter the distance between the lens and antenna to change the beam parameter entering the lens. After encountering the curved face of the lens the beam will again propagate through a constant medium, now HDPE, until it reaches the flat interface. So by changing the thickness of the lens, we are able to change the beam that must be created by the curved interface.

While it is a possible variable, increasing the thickness of the lens is not something we want. The beam is focusing in the lens, so increasing the thickness will require a larger beam at the curved surface. Since we are limited by how large our optics can be to begin with, we do not want the lens to be any thicker than necessary.

This leaves us with two variables to change. The beam leaving our antenna has a complex beam parameter of

$$z = .00241795 + .0092288i \tag{3.20}$$

By moving the antenna back from the lens we can increase the real term for the beam as it encounters the lens. We already know what the beam parameter will be after the curved interface. We can use this to find the spot size of the beam just as it leaves the

curved interface. While the curvature will affect the beam waist and angle of divergence, the spots size should not change immediately after encountering the lens. This means that we want to put the antenna far enough from the lens that the beam has expanded to the size we have calculated for the beam just after it enters the lens.

This leaves us with only the radius of curvature of the lens as the last remaining variable. The ABCD matrix for a curved interface is given by

$$\begin{pmatrix} 1 & 0 \\ \dfrac{n_2 - n_1}{n_2 R} & \dfrac{n_1}{n_2} \end{pmatrix} \tag{3.21}$$

where

R is the radius of curvature

n_1 in this case is free space

n_2 in this case is HDPE

It is a now an algebra problem to solve for the R which creates our desired beam. In our case, this radius of curvature is 6.9596 cm and the horn must be 14.2 cm away from the lens.

3.9 One Lens vs. Multiple Lenses

With the approach we have just taken, where diffraction is ignored, we will always find a solution to the problem which allows us to create whatever beam we want with a single lens. One of the downsides of the optical software that we used is that it works strictly from the formulas I have shown. There are many real situations where a second or even a third lens is necessary. These situations are the result of the physical limitations that lens curvature puts on the lens diameter.

As we have already seen, one of the primary concerns we were faced with was the diameter of our lens. We were only given 14 cm when we would have liked closer to 20

cm. When I solved for a lens curvature following the algorithm in the previous section, I arrived at a radius of curvature just under 7 cm. Obviously, it is not possible to have 20 cm diameter lens with a radius of curvature less than 7 cm. In such an event, we are now faced with the necessity of an additional lens. While the first lens may not focus the beam as much as we will eventually need, it can create a more collimated beam, which a second lens is capable of turning into the beam we are looking for. Any number of lenses would not have remedied our concern in this particular experiment. Unless we were able to use a large second lens, we would still be faced with the same concerns.

4. Refractometer

Density measurements taken with an interferometer can be used to find the average density over the path being sampled. The goal of the refractometer is to give a more thorough description of the density profile of the plasma. In a polywell fusion device the distribution of particles is extremely important.

In order to map the density profile we need to be able to send the beam through different chords of the plasma. While this could be done with the interferometer, a problem arises when trying to collect the beam. With the exception of the central chord, any other path will encounter density gradients that are not strictly perpendicular to the direction of propagation. As a result, without knowing the density profile beforehand, it is impossible to predict the location and direction of the beam exiting the plasma.

Unlike the interferometer, which has a single receiving antenna, our refractometer has an array of receiving antennas. Instead of analyzing the phase of the received signal, each antenna is attached to a detector which measures the power of the signal. This array allows us to take measurements without guessing where to place a single receiving antenna. The challenges that arise when considering the problem with Gaussian optics are presented in the next chapter.

4.1 Geometric Optics

While the wavelengths we are dealing with are too large for us to treat our beam with geometric optics, we can use it to show the goal and general behavior of the refractometer. In geometric optics, waves are treated as a collection of rays, each of which behaves independently from the other rays. When a ray encounters an interface across which there is a change in the index of refraction, the behavior of the ray changes.

42

Interaction normal to the interface will simply change the phase velocity of the wave. If the interaction occurs at any other angle, then the new wave will change according to Snell's Law:

$$n_1 \sin \theta_1 = n_2 \sin \theta_2 \qquad (4.1)$$

where

n_1 is the index of refraction in the first medium

n_2 is the index of refraction in the second medium

θ_1 is the angle between the direction of propagation of the ray prior to reaching the interface and the normal of the interface

θ_2 the angle between the direction of propagation of the ray after reaching the interface and the normal of the interface

As discussed in Chapter 3, the index of refraction encountered in a plasma depends on the wavelength of the signal, the density of the plasma, and the mode of the wave we are considering. In our case we are assuming waves in O-mode. Since our frequency is controlled, changes in the index of refraction are indications of a change in electron density. By measuring the position of the ray at our observation window, and using the relationship given in equation 4.1, it is possible to find information about the density profile encountered by the beam.

Figure 4.1 shows how rays will react to different density profiles for two plasmas which are both 18cm in diameter. Simulating a plasma with a constant density simply requires a single spherical lens with an index of refraction equal to that found in the plasma being modeled. In order to simulate a plasma with a Gaussian density distribution 15 nested spherical lenses were used. The index of refraction for each
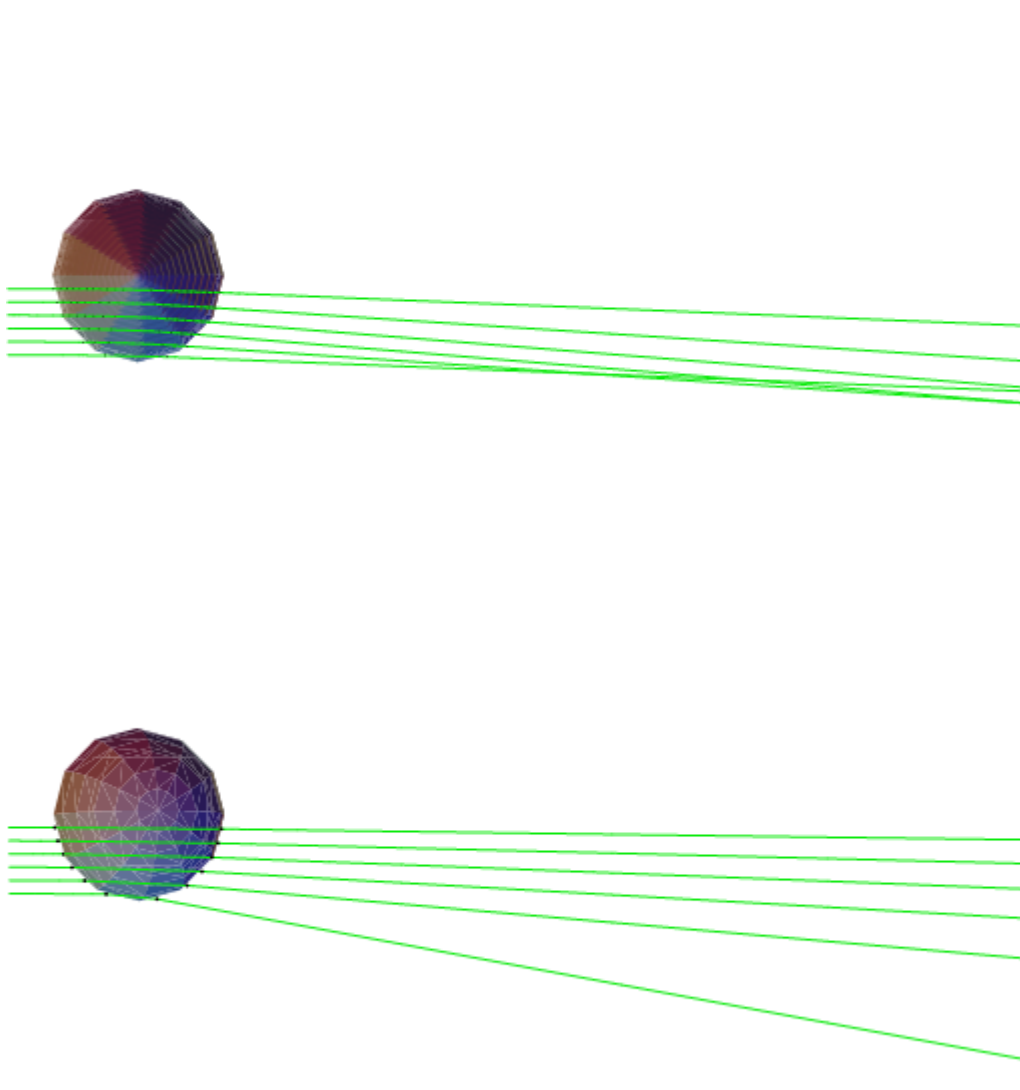
Figure 4-1: The behavior of rays as they pass through a plasma with (a) Gaussian density distribution and (b) constant density. The plasmas are both 18 cm in diameter and the screen is 1 meter from the center of the plasma.

Ray Source position (cm from center)	Ray position a receiver for Gaussian plasma (cm from center)	Ray position a receiver for constant plasma (cm from center)
8.307692	12.536	24.44688
6.923077	11.3421	14.25201
5.538462	12.57674	10.21038
4.153846	10.9651	7.245692
2.769231	8.298831	4.684458
1.384615	4.748178	2.305207

Table 4-1: For rays sent through the plasma at different distances from center the position of the beam when it reaches the edge of the chamber is given.

smaller sphere represents a plasma with a higher density. The result is a discrete version of what the beam will encounter as it travels along a density gradient. An interferometer output for both plasmas will show a line average density through the center of $\sim 1.41 * 10^{13} cm^{-3}$. In spite of this similarity, the two plasma's have very different density profiles. The first has a constant density over the entire plasma. The second has a Gaussian distribution with a peak density of $2.0 * 10^{13} cm^{-3}$ at the center. In Table 4.1 it is clear that the refractometer output for these two plasmas will be quite different. The direction of refraction (away from the center of the chamber) results from the fact that plasma, unlike most other materials, can have an index of refraction less than one.

It is also important that each of these rays can be collected by our refractometer. Of the 12 rays shown between the two plasmas, 11 will exit through the main observation port and the final ray will exit through the smaller side port. Provided that the plasma isn't much larger than expected, geometric optics predicts that our refractometer should be able to collect data.

4.2 Actual Circuit

While the system as a whole is less complicated than the interferometer, the refractometer Gunn circuit is more complex. Figure 4.2 shows the Gunn circuit that was built. The refractometer is designed to transmit waves with a frequency of 136 GHz. This keeps us safely above the plasma frequency while also being easily differentiated from our 94GHz interferometer signal.

The Gunn we used operates at 68GHz. The signal is then amplified and put through a frequency doubler, leading to our desired 136GHz beam. Using the doubler causes much of the increased complexity of the circuit. Putting a signal into the doubler

before it is properly biased can damage it. So in addition to carefully regulating voltage
throughout the circuit, power is not supplied to the amplifier until the doubler is biased to
-24VDC. The power in the transmitted wave approaches 200mW. Having such a strong
signal should allow us to detect even the lower intensity portion of our Gaussian beam
and give us a better picture of the shape of the beam we are receiving. In order to
produce this signal, the Gunn draws nearly 2A.

4.3 Space Concerns

In order to maximize the data gathered in each shot, the goal of this experiment is
to have the interferometer and refractometer channels working simultaneously. If we
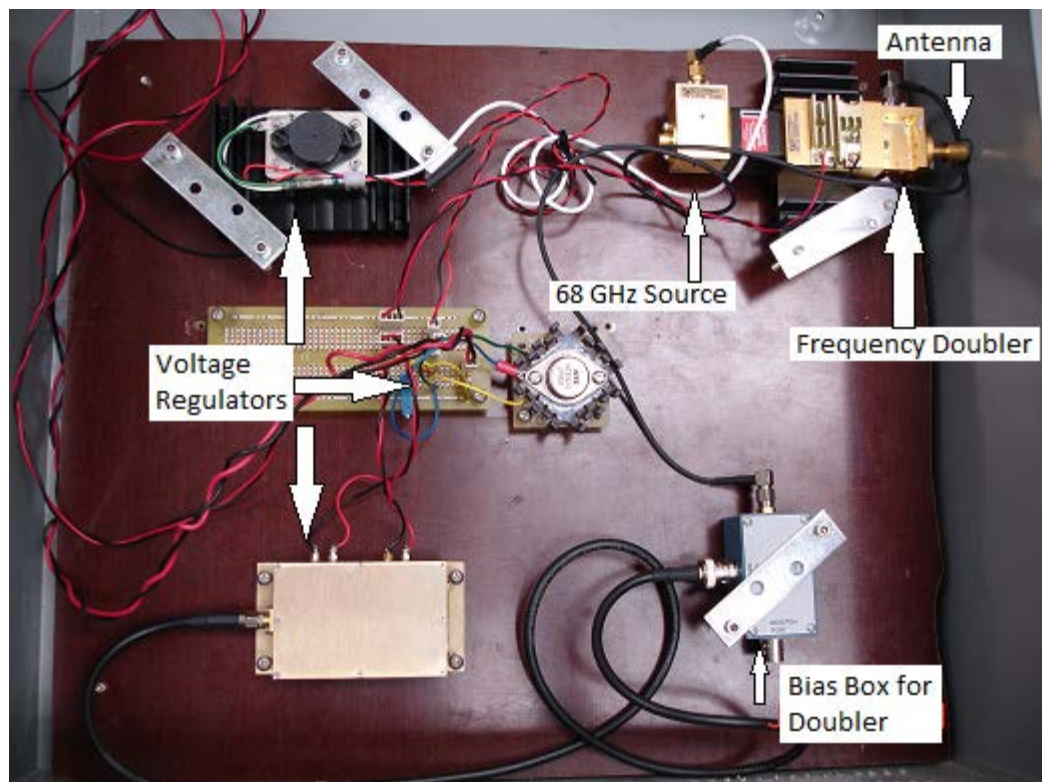were working in the geometric optics limit, this would not be a problem. A more

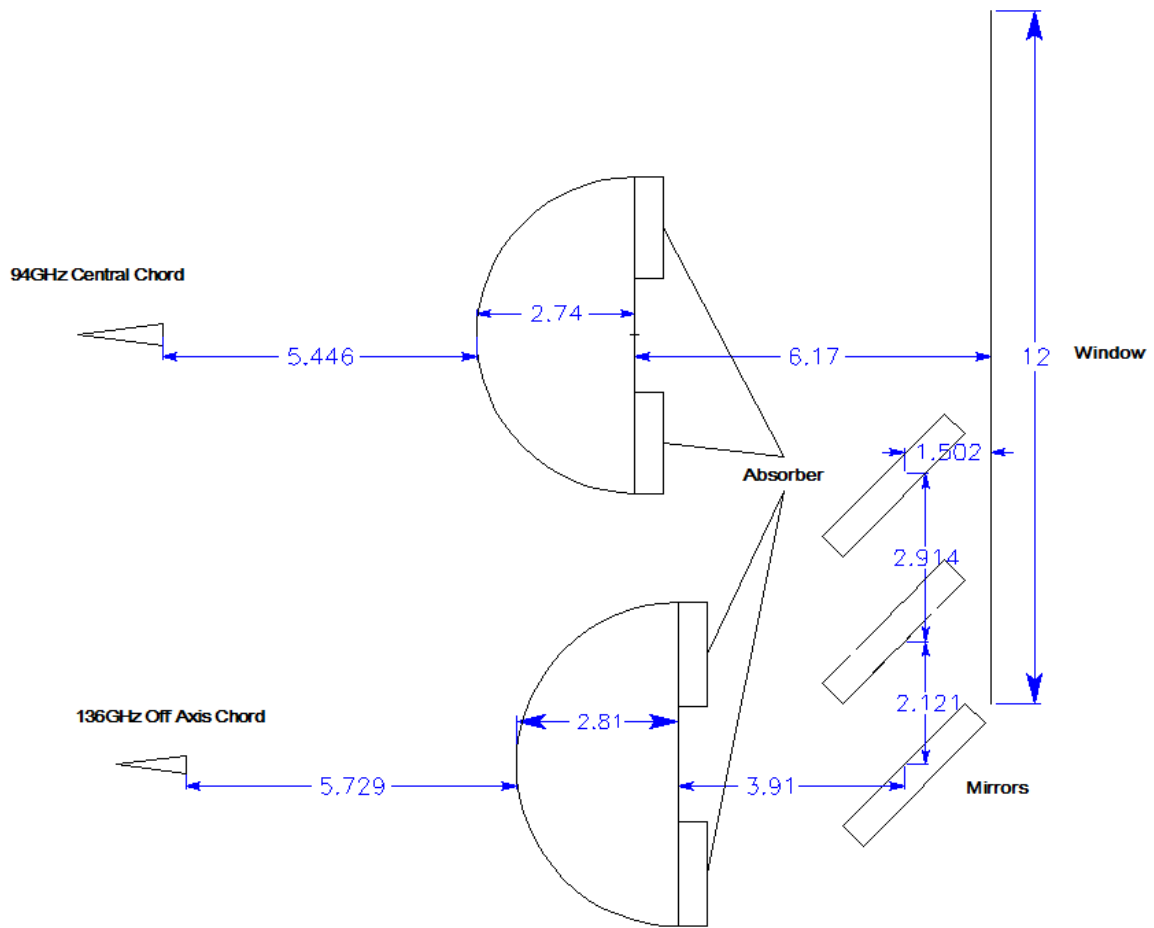**Figure 4-2: The refractometer Gunn circuit that was built**

46

Figure 4-3: Front end optics including both the interferometer channel and the refractometer channel with a translating mirror (units in inches)

compete discussion of the limitations caused by Gaussian optics follows in the next

chapter.

In order to maximize space, the decision was made to ignore diffraction for both

channels. Figure 4.3 shows the layout of the front end optics that was used. After

passing through the lenses, the beam from each channel is apertured to create a beam

with a diameter of 2 inches. While there was consideration given to aiming the

interferometer beam at an angle across the center of the plasma, it was decided that a

beam sent straight through will encounter a more symmetrical plasma.

Rather than move the entire refractometer Gunn when sampling different chords, the Gunn is located to the side of the viewing port and a mirror at a 45 degree angle directs the beam parallel to the window. The only moving part is a second mirror which directs the beam through the window, parallel to the original beam. This setup will allow for a range of motion of nearly 7.5cm for the center of the refractometer beam.

An advantage to using Gaussian optics is that it allows us model the shape of the beam despite the fact that we are unable to collect much of the signal. Figure 4-4 shows the receiving end of the chamber. The main viewing port has seven antennas shown. The antenna in the center of the window will also collect the signal for the interferometer. There are spaces between the antennas where a single ray could go undetected all together. In particular between the main window and the small side window, shown with three antennas, a narrow
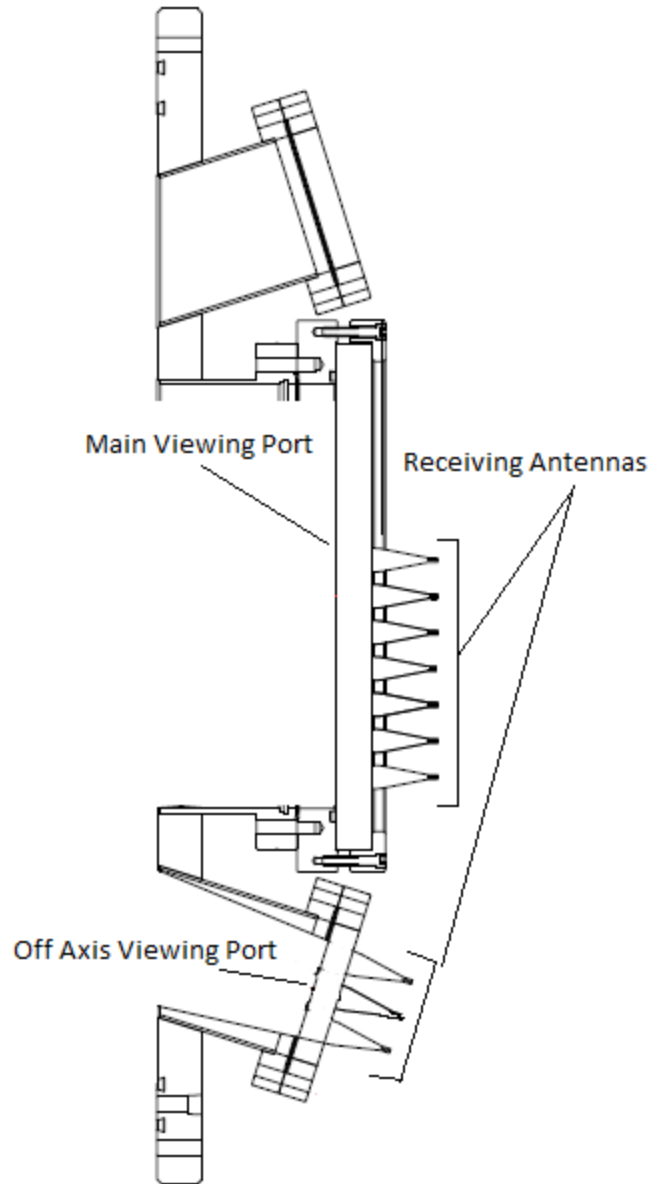
Figure 4-4: Receiving wall of the chamber with 7 antennas on the main port and three on the smaller viewing port.

beam could be easily missed. In ray tracing, the behavior of one ray is treated

independently from the rest of the signal. This makes it challenging to use the received

power to interpret the behavior of the rest of the beam. If the beam maintains a Gaussian

distribution, the relative power of the beam between detectors can be more accurately

approximated.

5. Bench Testing

There were two different approaches to bench testing the interferometer. From a purely practical point of view it is important to align the front end optics to maximize the power received by a circular horn antenna located two meters away. But beyond the particular application of our system, I also tested the behavior of the beam as the positioning of the front end optics changed. This provides a more thorough description of the beam as it passes through the plasma. It also helps illustrate the effect that diffraction has on the beam and how well it can still be modeled using Gaussian optics.

On one end of the test setup was the transmitting antenna on a translation stage. In front of that was the lens, which could be tilted as well as translated horizontally and vertically, shown in Figure 5-1. T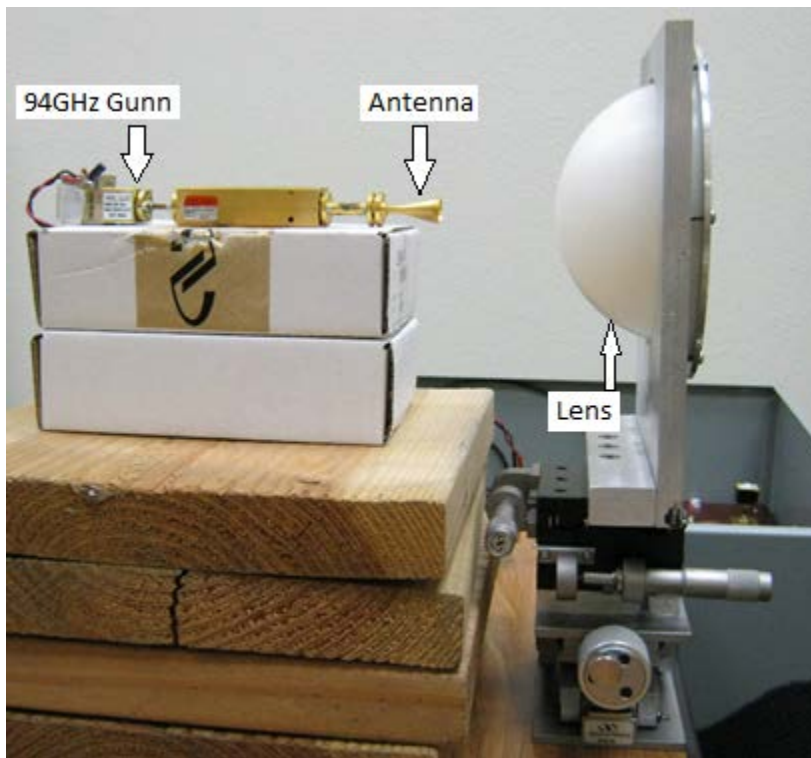wo meters away was the receiver. When evaluating the system for the sole purpose of maximizing the power detected, the receiver was the horn antenna that will be used in the actual system. When the goal was to obtain a more thorough description of the beam itself the receiver was an open ended WR-10

Figure 5-1: Launch end of bench testing optics

waveguide. The receiver was mounted on a pair of translation stages that allowed us to examine the full E-plane and H-plane fields of the received signal, shown in Figure 5-2. In every case during the testing, the difference between the E-plane and H-plane was minimal. The plots I have included in this chapter show simply the E-plane for this reason.

5.1 Horn Antenna

Before introducing the lens to the system, I first verified that the signal leaving our corrugated horn antenna was the beam we were expecting. To achieve this, I took measurements of the intensity of the beam at three locations; 1.5, 2.5 and 3.5 cm from the aperture of the antenna. For the horn used the theoretical complex beam parameter is $.002417 + i.0092288$. Figure 5-4 shows the plot of the theoretical beam distribution at each distance overlaid with the measured values. The measured points were taken with an open-ended waveguide moved in increments of quarter centimeters. These measurements verified that the physical beam is well modeled by the Gaussian beam we were predicting.
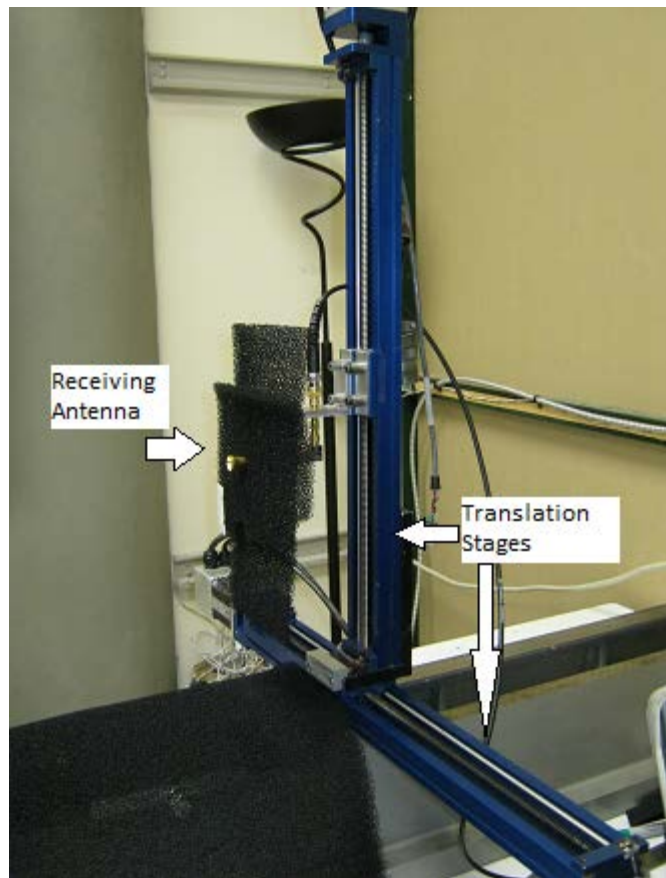

Figure 5-2: Receiving end of bench testing optics

51

5.2 Detector

There were two methods used to detect the signal. Initially a diode detector with its output read by a voltmeter was used. Until it is saturated, a diode detector's output will be a voltage that has a square-law scaling relative to the input power. In order to examine the shape of the beam, it is sufficient to find the relative power over the E and H-planes. For the practical use of the interferometer, it is useful to know the actual power received as well. In order to scale the diode detector I connected it through a series of couplers to the Gunn oscillator. The Gunn had a measured power output of 17dBm. By using different combinations of 3dB, 6dB and 10dB couplers, I recorded the detector outputs for different known power inputs. Figure 5-3 displays a log plot of the measured values, showing the operating region of the diode in addition to
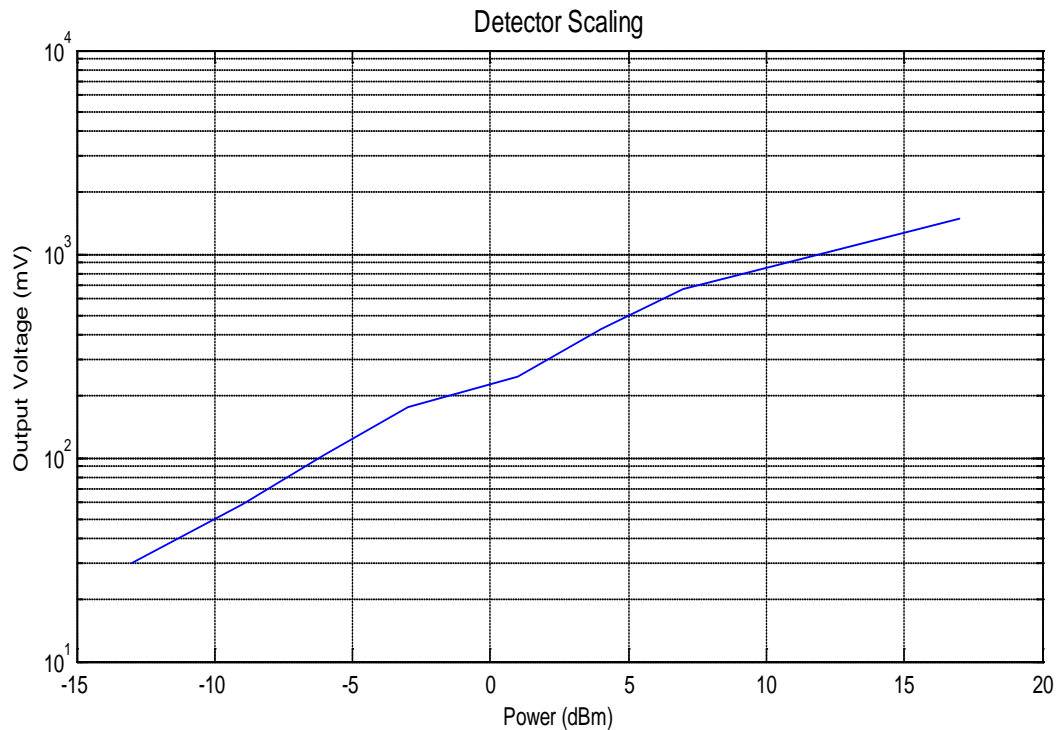

Figure 5-3: Scaling of the detector by measuring the output voltage while a beam with a known power is applied.
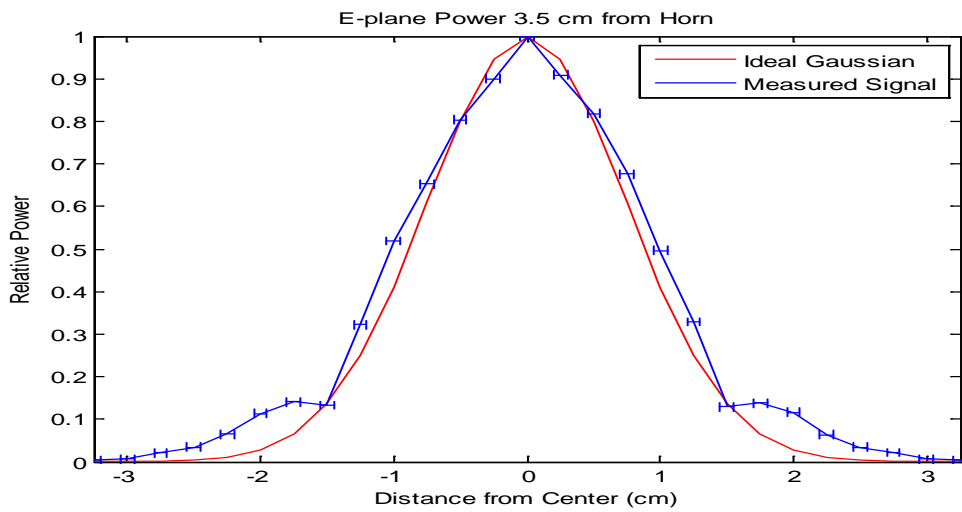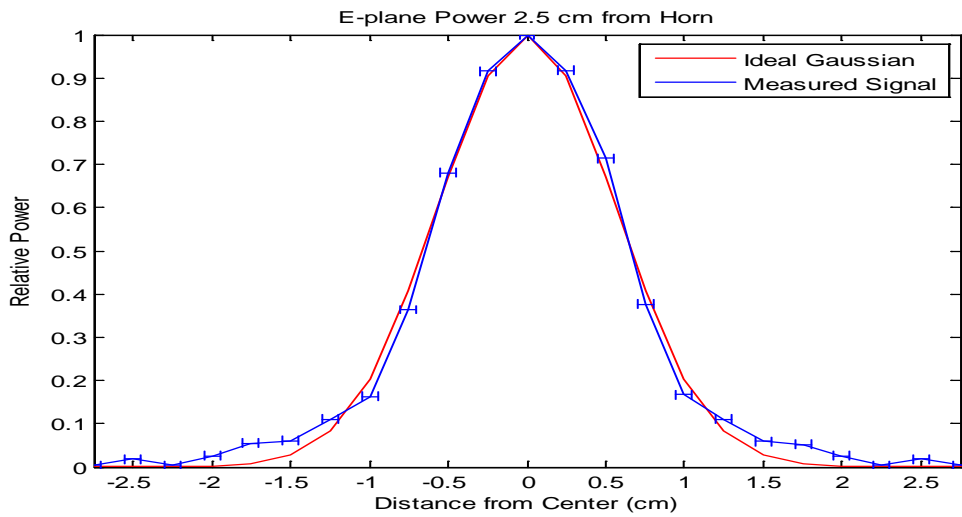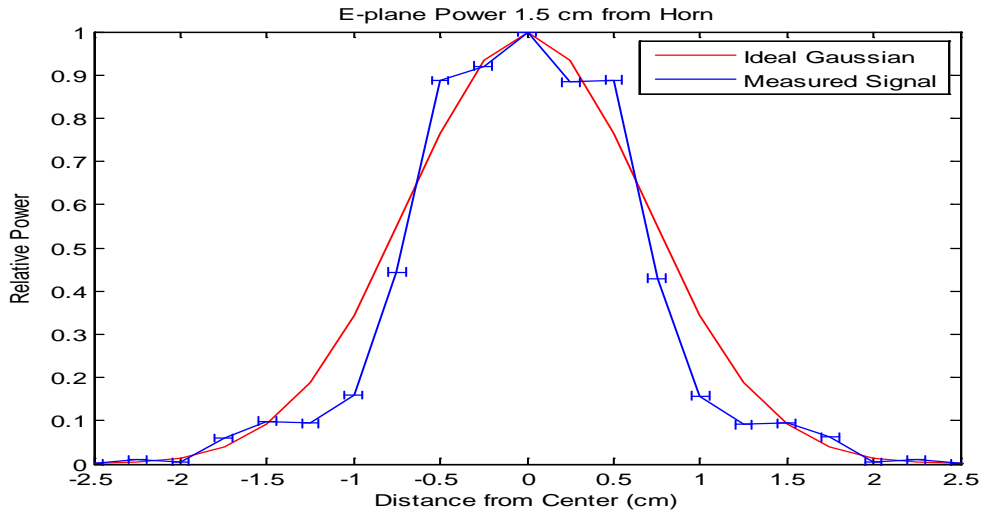
Figure 5-4: Beam profile of the actual beam leaving the antenna compared to an ideal Gaussian beam.
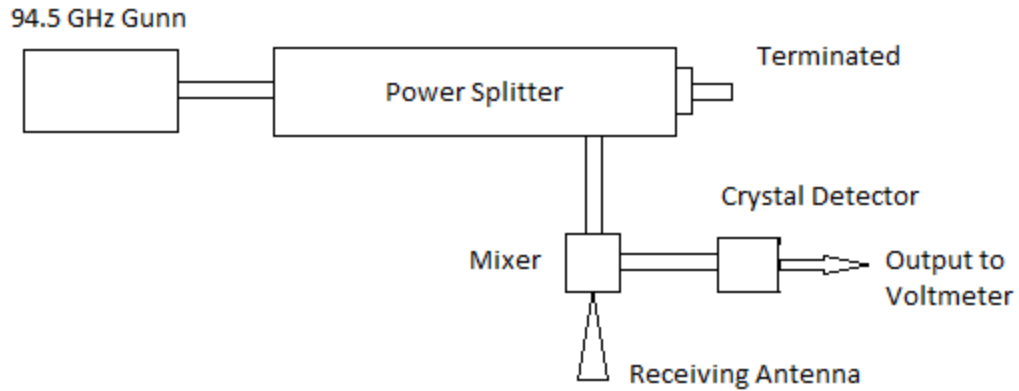
Figure 5-5: Schematic of mixer used as relative power detector

providing reference values for the diode output. When we aligned our antenna and lens to maximize the power received 2 meters away, the largest output we measured was 137mV. This corresponds to roughly –4.2dBm. The majority of this chapter will be more concerned with an examination of the shape and behavior of the beam. Maximum received power is a practical measurement of the system. Unfortunately the diode detector stopped working halfway through taking the measurements. Figure 5-5 shows the system used to replace it. Now the received signal is mixed with the attenuated signal from the other Gunn oscillator. This will have an output of approximately

$$\frac{A_1 A_2}{2} \cos 500 MHz$$

where A_1 is the constant power from the Gunn and A_2 is the varying power from the received signal. The output of the mixer was then sent through a crystal detector, giving us

Figure 5-6: Mixer used as a detector after the original detector failed.

an output similar to the original diode detector. It isn't important to know the actual power received when examining the shape of the beam, the relative power is sufficient. For this reason I did not scale this detector as I did for the original diode detector since I already had the only scaled power measurement that I needed.

5.3 Examining the Optimum Beam

As an extension of the practical part of this experiment, before looking at a range of other beams, it is helpful to examine the behavior of the beam that delivered the maximum power to our receiver. Figure 5-7 shows the actual beam that created our strongest signal. This was measured at different points along the path, with the two most important points being the center of the chamber and the receiving end of the chamber.

To find the spot size of the beam 2 meters from the lens, we need to find where
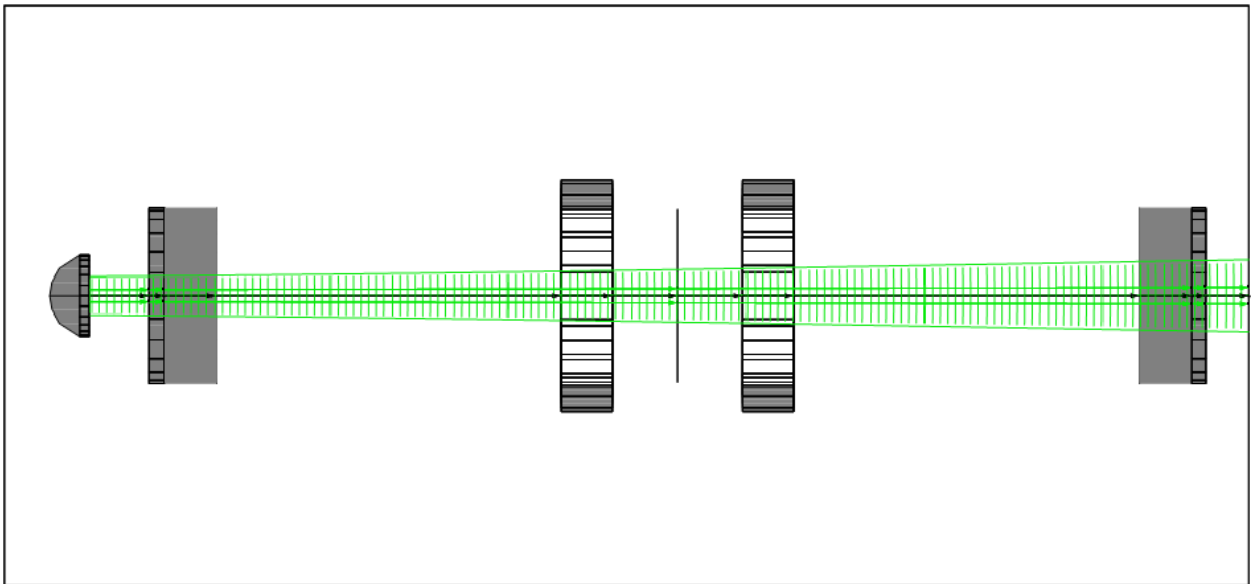
Figure 5-7: Actual Measured Gaussian Beam

the relative power drops to 13.5% of the central beam power or e^{-2}. For our beam the spot size is 7.5 cm. Figure 5-8 shows that the beam I measured is nearly identical in shape to an ideal Gaussian beam with the same spot size.
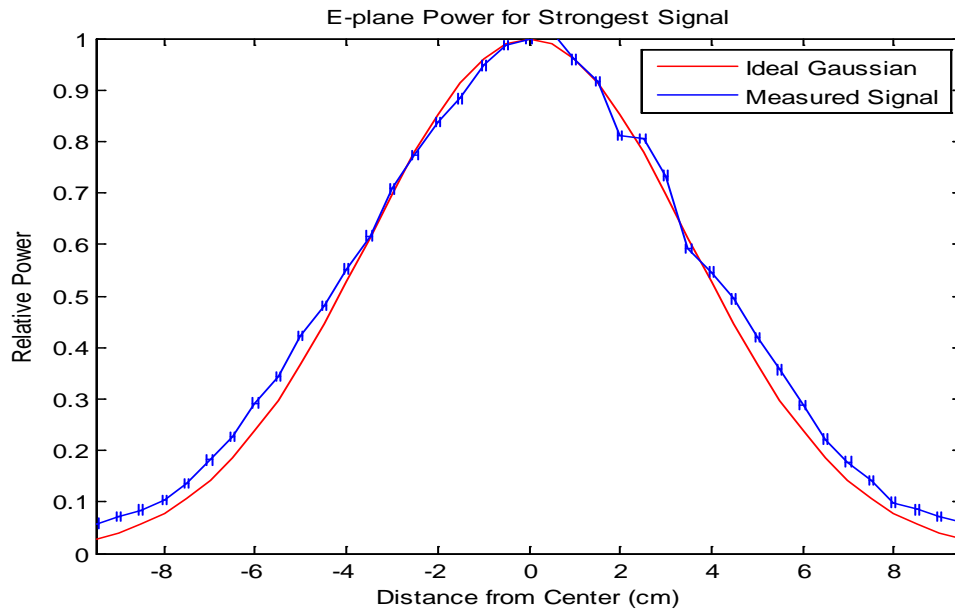
Figure 5-8: Measured beam profile of the strongest received beam compared to an ideal Gaussian beam

In addition to examining the correlation between the measured beam and an ideal

beam, I also needed to verify that the power at the center of the beam was consistent over

the full distance that the beam propagates. Based on the power measured at the center of

the beam 2 meters from the lens we can calculate what the peak values should be at every

point along the beam. Figure 5-9 shows the beam that was measured at the center of the

chamber, 1 meter from the lens, as well as the expected beam that would be consistent

with our 2 meters measurements. We can see that the beam correlates strongly and that

the entire beam behaves like the beam shown previously in Figure 5-7 which is described

by the beam parameter $z = .472 + i1.43827$ leaving the lens.

In order for diffraction effects to be negligible in Gaussian optics it is ideal to

have the diameter of all apertures be four times the spot size of the beam passing through

it. By the time the entire beam has hit the lens for the optimum beam, the spot size is

barely half the diameter of the lens, so we knew beforehand that diffraction would be a

concern. It is very positive to see that while significant power is lost, and the beam is

	Theoretical	Measured
Beam Parameter	.3617+i.1101	2.42+i1.438
Beam Waist	1.058 cm	3.82 cm
Spot Size at Receiver	22.3 cm	7.5 cm
Power Received	.086mW	.38 mW

Table 5-1: Comparison between the measured signal and the theoretically expected signal.

quite different than it would have been without diffraction, we still are dealing with a beam that is well approximated by Gaussian optics. Table 5-1 shows the difference between the beam we expected if we ignored diffraction and the actual beam that was measured.

The amount of power lost is quite significant. For the aperture size we should expect to lose about 4% of the power in the beam as it passes through the lens. The initial beam has 50mW of power so we should expect the receiver antenna to pick up 0.7mW of power from a beam with a spot size of 7.5cm. Our antenna actually picked up 0.38mW of power which indicates that there is loss elsewhere in the system. While there was likely some power lost as the beam propagated through the lens and then 2 meters through air, it is also likely that diffraction increased the power in the side lobes outside
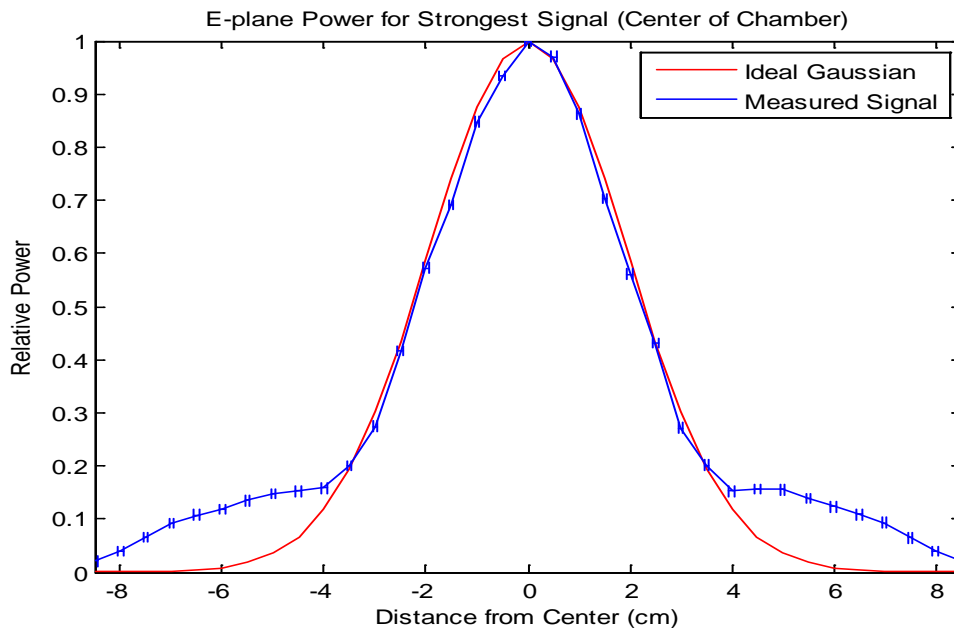

Figure 5-9: Measured beam profile of the strongest received beam when observed from the center of the chamber compared to an ideal Gaussian beam

57

the range of motion of our testing apparatus.

5.4 Diffraction

We expected diffraction to create beam profiles that differed from our models leaving us with two major questions to examine. The first is whether or not the beam can continue to be approximated using Gaussian optics. This will be crucial in the refractometer as we need to know the profile of the beam entering the plasma for the profile leaving the plasma to contain any information. Our second concern is how much power is contained in the beam's primary lobe. I examined both of these questions by measuring the beam profiles as I changed the spacing between the transmitting horn and the lens. A shorter distance results in a smaller beam entering the lens and, as a result, less diffraction.

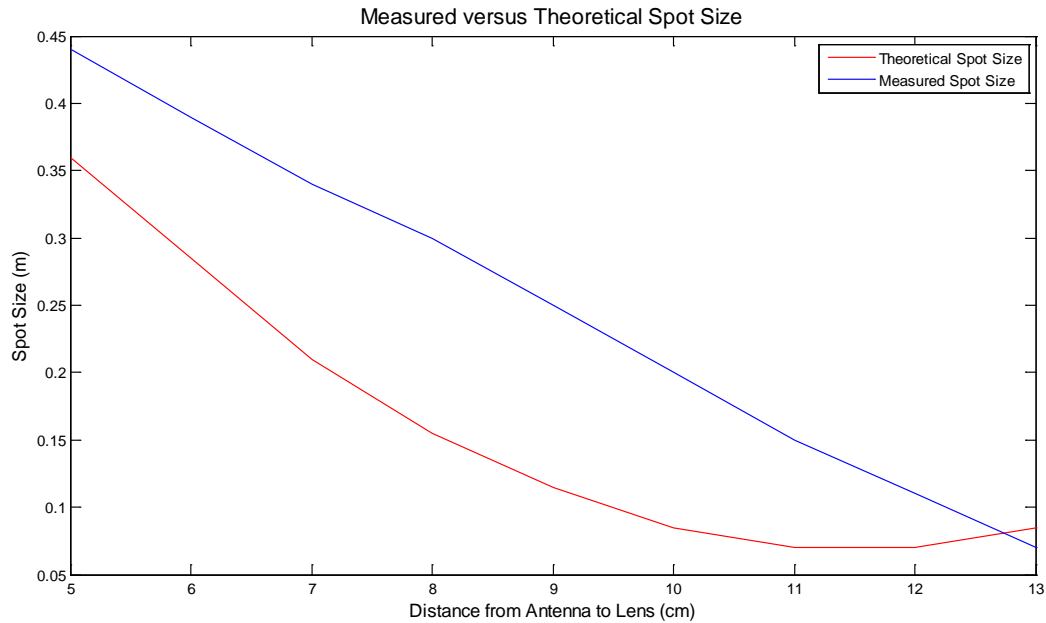When examining the optimum beam, we saw that this beam is well represented

Figure 5-10: Comparison of the measured spot sizes of different beams and the theoretically expected beams.
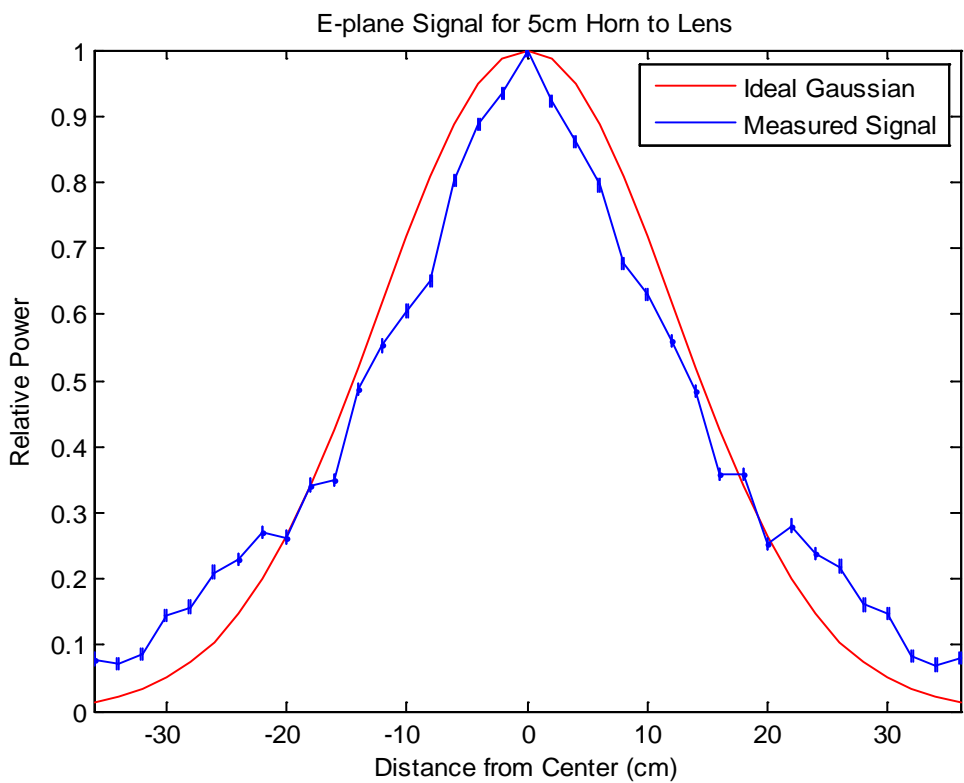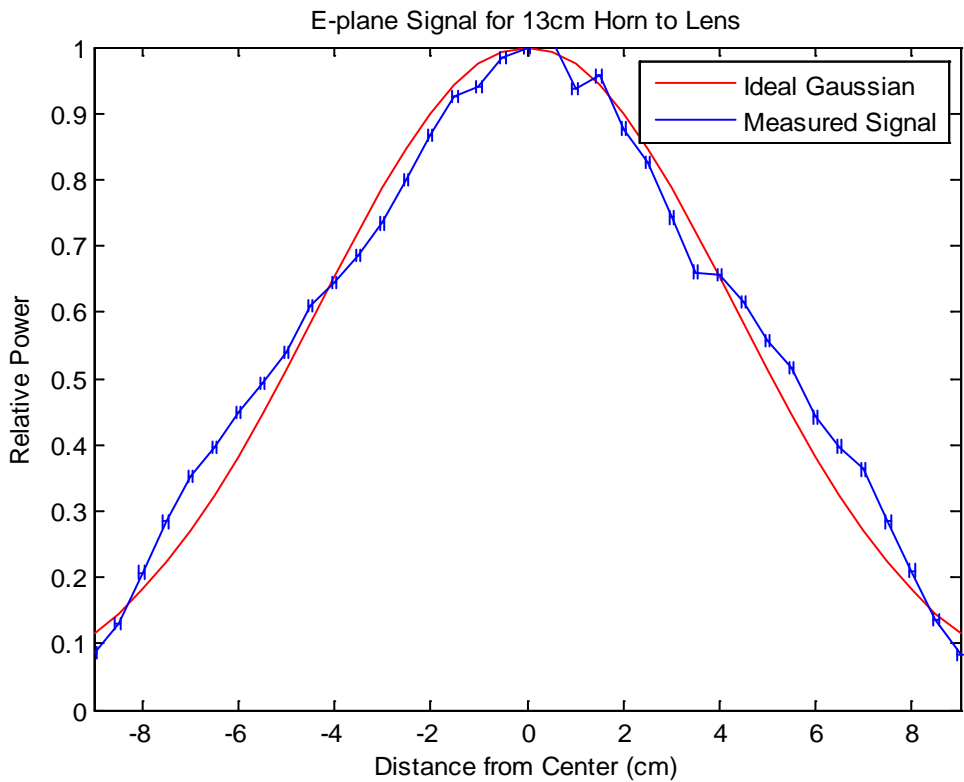
Figure 5-11: Beam profile at the receiving end on the chamber for the two most extreme beams measured; 5cm and 13cm from antenna to lens.

by Gaussian optics. In that case, the distance between the antenna and the lens was 9.4 cm. I also examined beams where this distance ranged from 5 cm to 13 cm. In each case, the profile of the beam was Gaussian. Figure 5-11 shows the profile of the beam 2 meters after leaving the lens for the two extreme cases, plotted with their ideal Gaussian profile. Again we see that the approximation still holds. This is great news for the refractometer as it shows that we may be able to aperture our beam while still operating in the realm of Gaussian optics. Figure 5-12 plots the spot size of our measured beam alongside the expected spot size. Even for a 5 cm distance between horn and lens, more than 7 cm less that our ideal model calls for, the shape of the beam is significantly altered.

While the main lobe of the wave continues to behave as a Gaussian beam, power is lost quickly when the beam spot size entering the lens is increased. Figure 5-12 uses

Figure 5-12: Approximate spot size of our measured beam compared with the expected theoretical power.

the 5cm spacing as a reference for the peak power of a beam with a given spot size. When we did this earlier in this chapter to look at our optimum beam, we accurately predicted the peak intensity at the center of the chamber based on the beam exiting the chamber. In the same way, Figure 5-12 shows what the peak intensity should be for each beam, based on the spots size. When the spacing is 6 cm the intensity is predicted almost exactly. By the time the spacing is up to 8 cm, the correlation is terrible. A valuable comparison is the 11 and 12 cm spaced beams. In both cases the spot size is 7 cm, but the 12 cm beam has only 85% as much power. The fact that the beam is larger entering the lens would only account for the 12cm beam containing 97% of the power in the 11cm beam. This means that there is a great deal of power contained in the side lobes.

5.5 Interferometer Circuit

Until the interferometer is connected to the actual polywell chamber, I won't be able to calibrate it in a meaningful way. Therefore, in order to verify that the circuit is working, I used a mirror to reflect the transmitted signal back to the receiving antenna. When the mirror is perfectly still the I and Q signals showed a DC value. Figure 5-13 shows the oscilloscope screen for two different scenarios. The image on the left shows the output when the mirror is moved slowly. In this case the signals have a low frequency signal. The image on the right shows a high frequency signal resulting from moving the mirror rapidly. In both cases the two signals are correctly 90 degrees out of phase.

Distance from Antenna to Lens (cm)	Power at Beam Center	Power 2.85cm from Beam Center
10	286	138
10.2	292	139
10.4	298	142
10.6	301	151
10.8	289	159
11	277	132
11.2	268	138

Distance from Antenna to Lens (cm)	Power at Beam Center	Power 2.85cm from Beam Center
16	81	57
15	110	65
14	144	85
13	186	111
12	234	148
11	277	132
10	286	138
9	167	95

Table 5-2: Measued beam strength at the beam waist and 2.85cm from the beam waist

5.6 Refractometer

The difficulty in predicting the refraction of a beam led to the use of a 200mW source to insure that there was enough power available at the receivers. While it would still be advantageous to have a Gaussian beam, two characteristics of the beam are more important. The first is that we want as narrow a beam as possible in the center of the chamber. Secondly, the beam needs to have a distinct center.

I took advantage of the fact that I had multiple 136GHz detectors in order to minimize the beam's size as it passes through the plasma. Instead of using a single detector 1 meter from the plasma, I used two detectors that were 2.85 cm apart. With on detector at the beam center, I was less concerned with the raw power in the center, and more concerned with the drop in power seen in the second detector. A
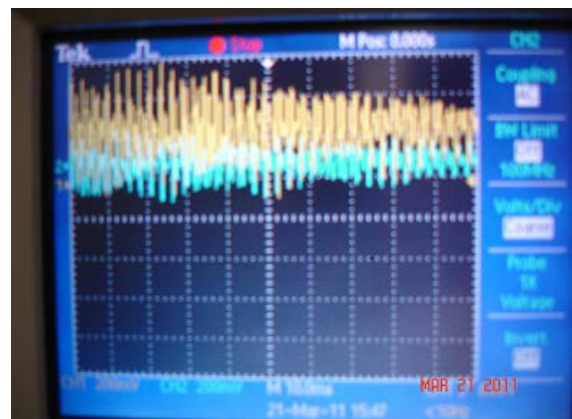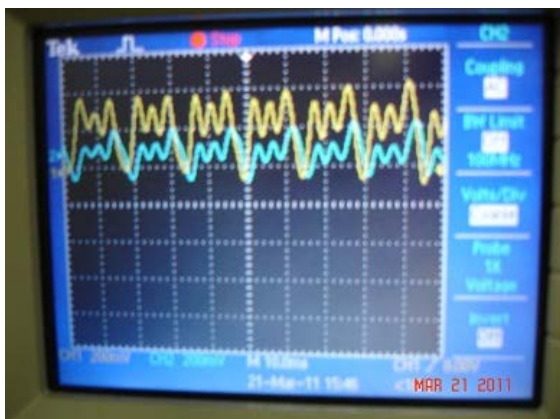

Figure 5-13: Oscilloscope output from the interferometer showing different rates of phase change.

quicker drop indicates a narrower beam. Table 5-2 shows the power in the two detectors as the distance between the antenna and lens changes. The narrowest beam occurs between 10 and 11cm. Testing solely in that region we see that the best beam occurs when the spacing is 10.2cm. This is also nearly the peak central power. A more complete testing of this spacing shows that the beam waist is 61cm into the chamber. Because the frequency is higher than the interferometer, the same size optics are now able to put the waist inside the chamber.

5.7 Mirrors

The real concern for the refractometer is how the beam will respond to being reflected off two small mirrors that will work as essentially 2 inch apertures. Figure 5-14 shows the beam profile 2 meters away from the last optical component when that component is the lens, a single mirror, or the second of two mirrors. As expected the
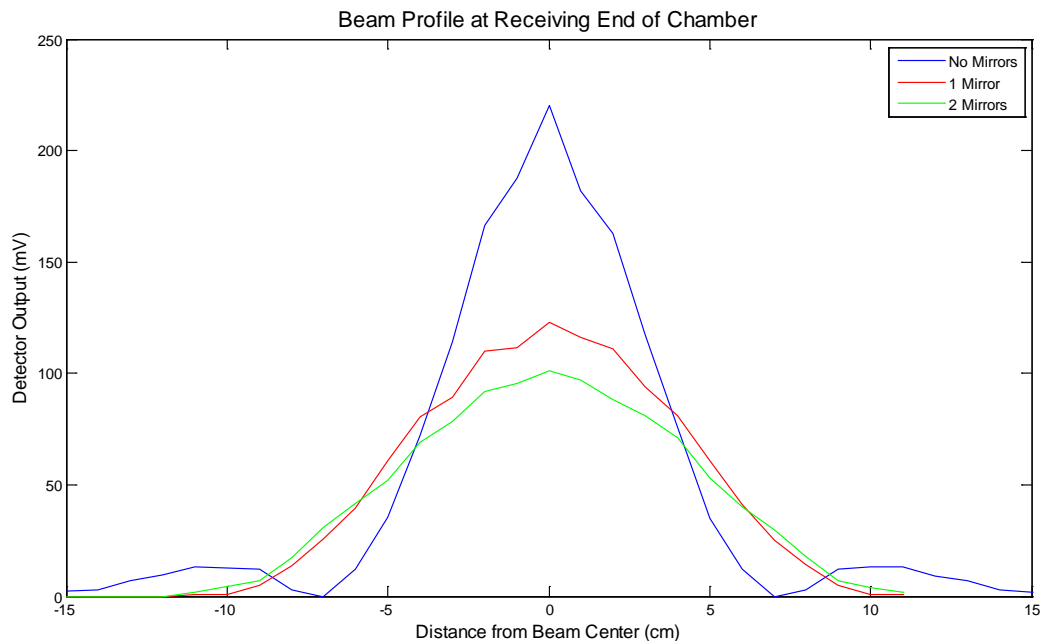
Figure 5-14: Comparison between the shape and power of beam at the receiving end of the chamber when the signal is aperture by a mirror once, twice, and not at all.

beam losses power and spreads out each time it is apertured. Fortunately, the power loss is not a major concern to begin with and, while the beam spreads out, there is still a clear beam center. Nevertheless, as a result of this test the front end optics are being redesigned to use a single mirror, rather than two.

6. Experimental Results

Once the interferometer was built it was attached to the WB-8 machine as shown in Figures 6-1 and 6-2. The receiving end of the chamber is shown in Figure 6-1. The interferometer box is mounted such that the receiving antenna is in the center of the window. Waveguide is used to guide the signal around the chamber to the front end, which is shown in Figure 6-2. The waveguide ends with a corrugated horn antenna which transmits the signal through the lens and into the chamber. This chapter will discuss the early plasma density results found using the interferometer.
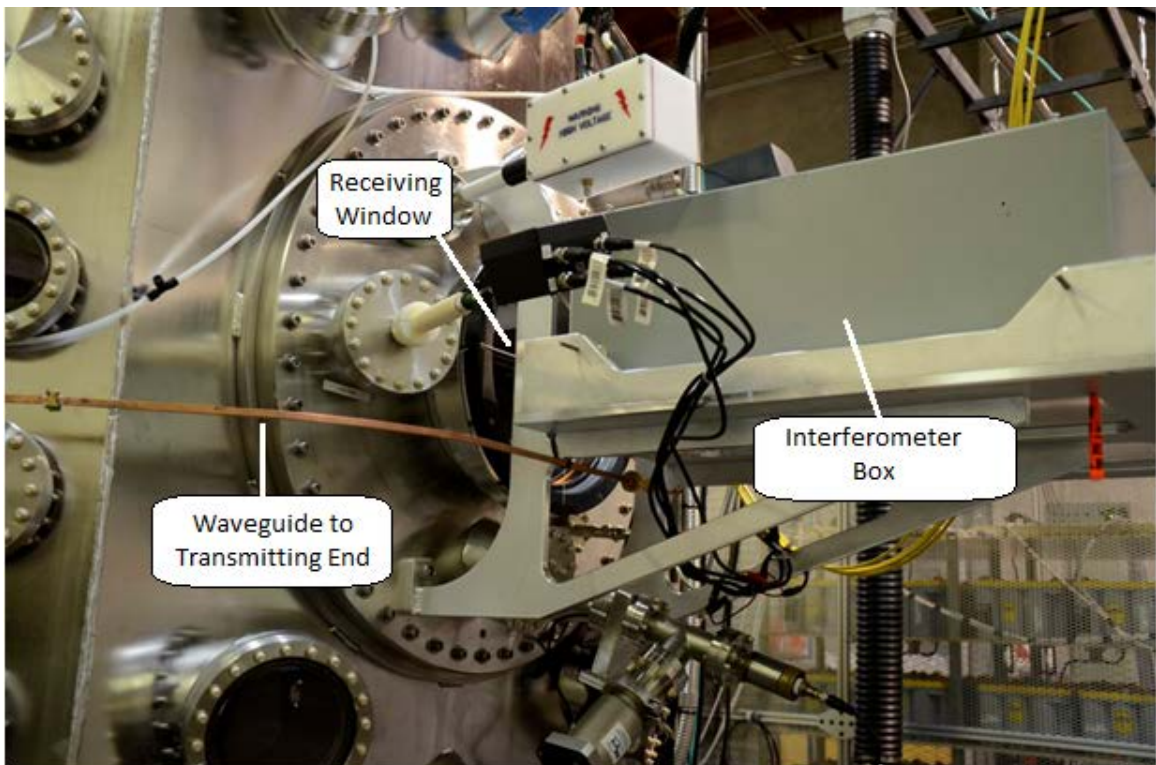

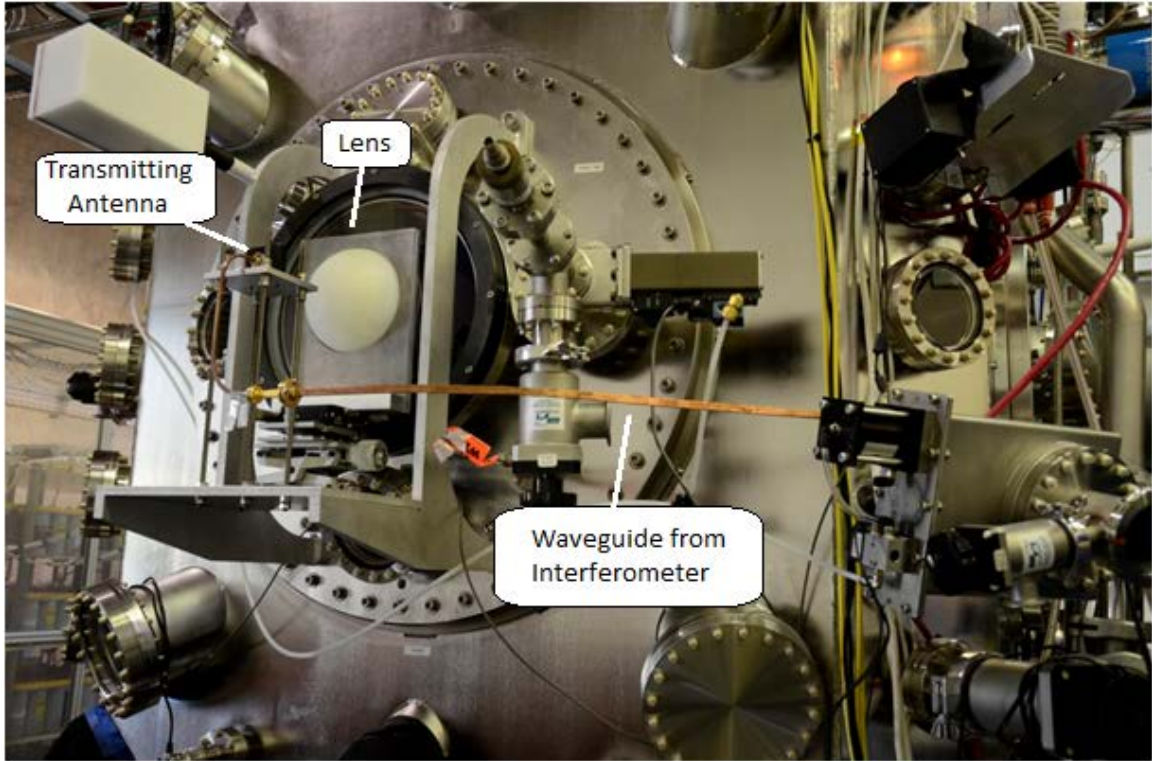**Figure 6-1: Receiving end of the interferometer system**

Figure 6- 2: Transmitting end of the interferometer system

6.1 Calibration

In order to calculate the plasma density from the I-Q signals, first we need to know the range of these signals. Both the I and Q outputs are sinusoidal. Calibrating the system requires us to find the amplitude of the signals, as well as any offset. This was done without a plasma in the chamber using the phase shifter built into the interferometer. The phase shifter changes the phase of the signal which propagates through the chamber. This clearly changes the phase difference between that signal and the reference signal. I was able to determine the amplitude and offset of the two signals, shown in Table 1, for the first set of measurements. Any time the amplifiers or attenuators are altered this calibration will need to be repeated.
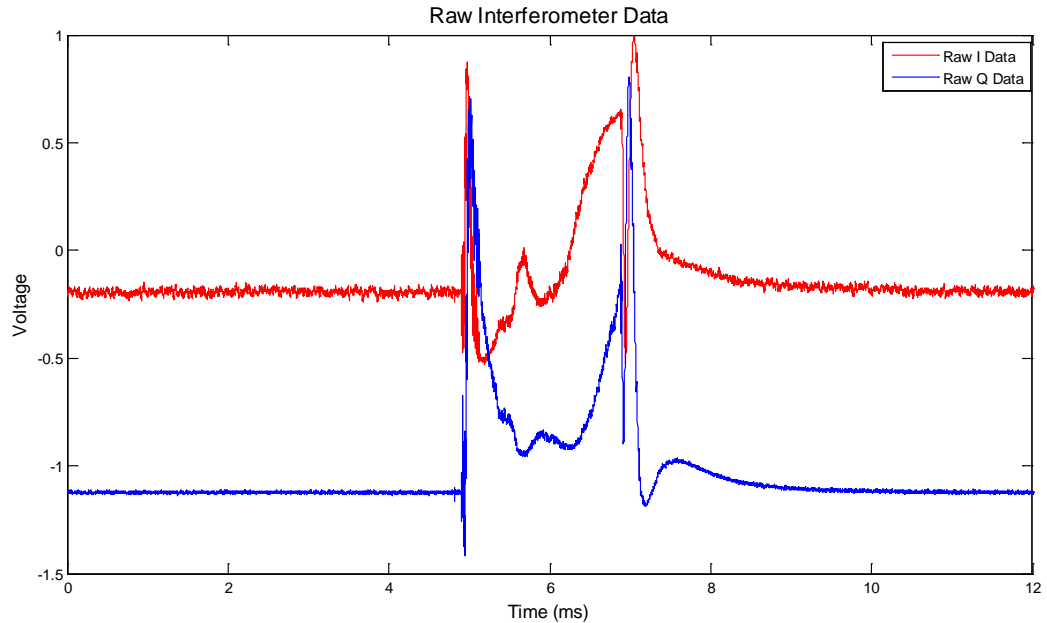
Figure 6-3: Raw I and Q signals from the interferometer during a 2ms plasma shot

6.2 Raw Signal

One of the first sets of data I was given to analyze was for a plasma created using a 2 ms shot from a plasma gun with all six coils on and a B-field of approximately 2 kilogauss. Figure 6-3 shows the raw interferometer output. Before and after the shot the two channels have a nearly constant signal. At the beginning of the shot, and again near the end, there is a rapid change in the I-Q outputs as the phase changes rapidly. In the middle of the shot there is some change, but it is less extreme. In order to remove some of the noise from the signal, a smoothed version was created and analyzed. A moving average was used to create the smoothed plot in Figure 6-4.

6.3 Line Average Density

Using the method considered in Chapter 2, these two interferometer outputs can be used to find a line average density for the plasma being measured. First, the I and Q signals are used to find the phase shift during the shot. Figure 6-5 shows the phase plot that is obtained from simply taking the inverse tangent of the I data divided by the Q data.

67
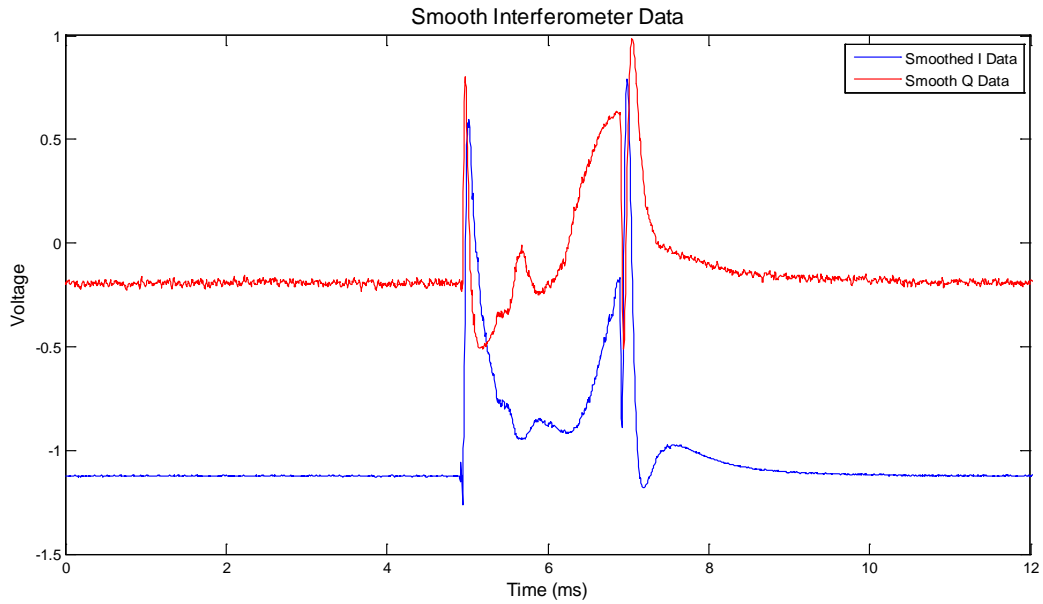
Figure 6-4: Smoothed I and Q signals from the interferometer during a 2ms plasma shot

Getting from the phase plot to the density is simply a matter of scaling and adding an offset. This plot seems to imply that the density of the plasma rose quickly, then almost instantly dropped to a lower density than we started with. The real cause of this rapid drop is that the inverse tangent function will not give a phase greater than π or less than –π. Once the phase became larger than π it loops back around to –π. In order to have a

Figure 6-5: Phase shift data from a 2 ms plasma shot

Figure 6-6: Line average density after eliminating fringe jumps from a 2 ms plasma shot (assuming a plasma diameter of 20cm)

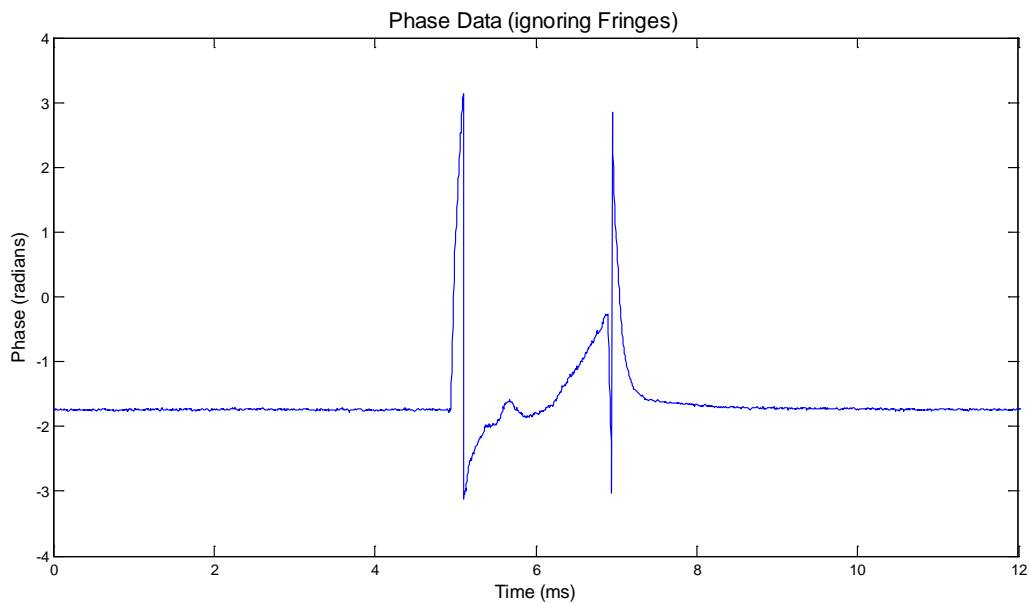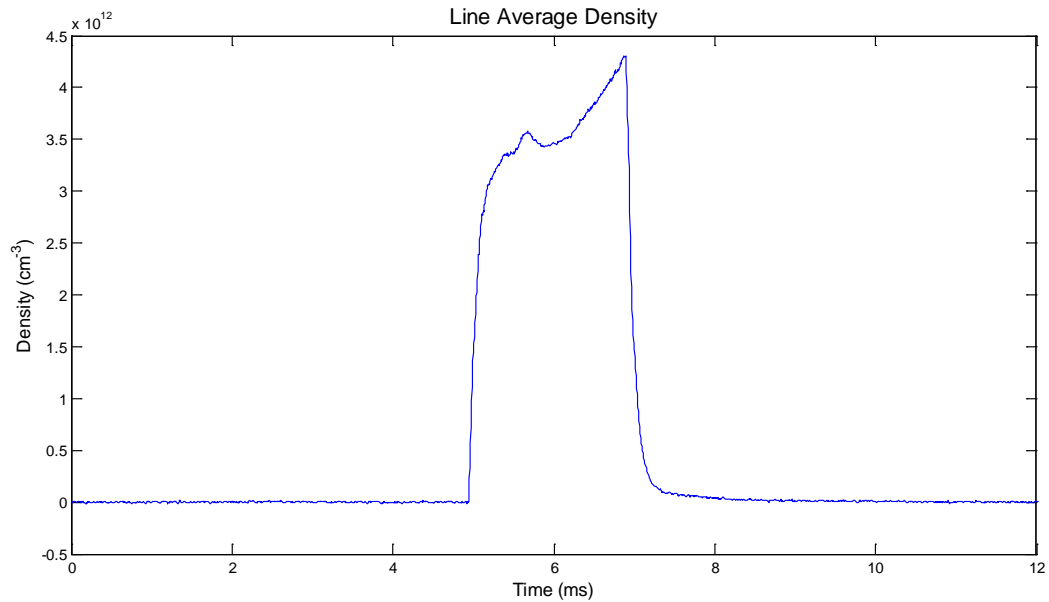meaningful density plot we have to differentiate between one of these fringe jumps and

actual phase changes. In order to achieve this, my code follows the method used in

[*Ejiri*]. The raw phase data is convolved with a short pulse. When a portion of the phase

data changes more rapidly than the surrounding data, the output of the convolution is

large. Changing the width and amplitude of the pulse changes the parameters of what is

considered a fringe jump.

Once the fringe jump is removed and the data is scaled the density plot can be

seen in Figure 6-6. The density has a rapid increase which slows for most of the shot

before rapidly decaying at the end. This particular shot used all 6 coils but no electron

gun. The coils will eventually be charged up to 25kV. For this shot the coils were not

charged. Assuming that the plasma is approximately 20cm in diameter, the peak density

is around 4.2e12 cm^-3.

69
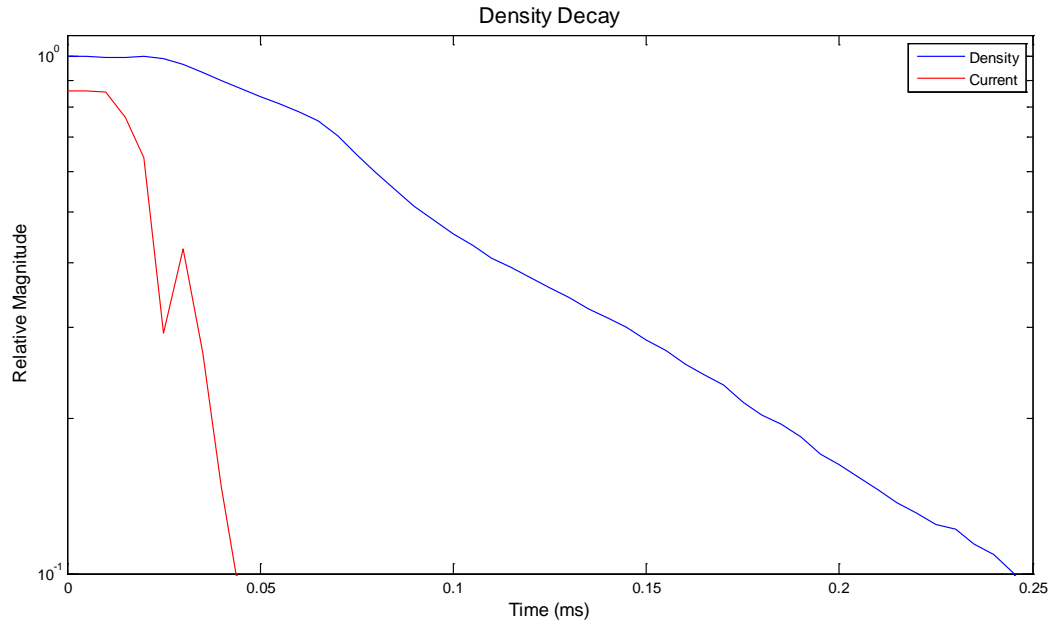
Figure 6-7: Line average density decay once the plasma source is turned off.

6.4 Density Decay

The most interesting behavior exists once the plasma source has been turned off. Until that point it is impossible to know what portion of the density to attribute to successful confinement and what portion results from simply adding more plasma to the system. Figure 6-7 shows the how the density decays next to the current from the plasma source. In addition to the peak density, the rate of decay in this region will give us a good idea of how well the plasma is being confined.

7. Conclusion

The 94 GHz interferometer mounted on EMC2's WB-8 chamber provides information about the line average density of a cord through the center of the plasma. This measurement is crucial for a fusion plasma, where density is a major limiting factor for the frequency of fusion events.

A heterodyne configuration was chosen for the interferometer in order to increase power in the system and to eliminate some ambiguity in the received signal. Unlike a homodyne interferometer, our system can detect the direction of a phase shift since it moves from 500 MHz rather than from 0. An I-Q mixer further clarifies the signal by decoupling signal changes that result from phase shifts, which we are interested in, from those caused by amplitude changes.

In order to test a chord through the plasma, a lens system was designed to transmit our desired beam through the chamber. Ideally, this beam should be as narrow as possible and collimated as it passes through the plasma. Modeling the beam was simplified by using a corrugated horn antenna which transmits an approximately Gaussian beam.

Gaussian optics were used to model the behavior of the beam as it leaves the antenna, passes through a lens and then propagates approximately two meters through the chamber to a receiving horn. Physical space limitations in the system prevented the use of a lens large enough that diffraction effects could be ignored. As a result, bench testing of the optical system was needed to ensure that the beam profile was understood. While diffraction changed the waist size of the beam, the profile remained Gaussian and very little power was lost.

Interpreting the density from the received signal requires solving the dispersion relation for the propagating waves. Interferometers are typically oriented with the beam travelling perpendicular to magnetic field lines. As a result O-mode waves are received which have a simple dispersion relation. The geometry of WB-8 makes it impossible to avoid sending the interferometer beam parallel to field lines. By choosing a high frequency the R and L mode waves can be well approximated by using the O-mode dispersion relation.

One major limitation of the interferometer is that it doesn't provide any information about the distribution of the density. A refractometer was also designed to give a more thorough picture of the density profile. The optics are similar to the interferometer, but the receiver is an array of horns with power detectors. The system has been designed but has not yet been used on the machine.

In many ways WB-8 is still operating well under capacity. The Marx Bank which charges the coils has been turned on, but only seven of the eventual 20 capacitors are connected. Even those seven capacitors have not yet been fully charged. The electron gun is being repaired and has not been used with the interferometer mounted. Density measurements from the interferometer will be vital as these and other systems are implemented. The measurements have already provided information about the plasma currently being made.

An important next step will be to complete and mount the refractometer. The optics are finished and all parts have been purchased and received. Once the scheme for mounting the system on the Polywell chamber is finalized I can begin to wire the receiving array. The Gunn oscillator is already wired and ready to be mounted. While

there will be challenges in interpreting the density profile of the plasma even with the Refractometer, it should be possible to get a better sense of the size and profile of the plasma being measured.

PARTS LIST

OPTICS	Quantity	Vendor
U100-P Precision Platform Mirror Mount	2	Newport Optics
UPA-PA1 Horizontal Adaptor	2	Newport Optics
SP-2 Standard Post	2	Newport Optics
SP-1 Standard Post	2	Newport Optics
VPT-2 Translating Post Holder	2	Newport Optics
PRL-12 Precision Optical Rail	1	Newport Optics
PRC-1 Rail Carrier	2	Newport Optics
AJS100-0.5K Adjustment Screw	4	Newport Optics
M-EL80 Lab Jack	2	Newport Optics
TGN80 Tilt Platform	2	Newport Optics
423 Linear Stage	2	Newport Optics
High Density Polyethylene Lens	2	

INTERFEROMETER		
94.0 GHz 17 dBm Gunn with isolator (0.6 db)	1	HXI
93.5 GHz 17 dBm Gunn with isolator (0.6 db)	1	HXI
10 dB directional coupler	1	Hughes
Balance mixers (93-95 GHz), 110-13 dBm LO power with IF amplifer (0.1 - 1GHz)	2	Millitech
Attenuator (0-20 dB) set screw	2	Hughes
0-180 degree phase shifter	1	Millitech
3 dB coupler	1	Baytron
Corrugated Horn antenna - Lauching at 94GHz	1	Millitech
3 dB power splitter	1	Millitech
Various waveguides + flanges, screws	1	Penn Engineering
Low frequency mixer and baseband amplifer	1	Mini circuit
Band Bass filter - 8921Z	1	Pacific Millimeter
IF amplifiers (351A-3-4.7-NI)	2	Analog Modules
Horn antenna - Receiving at 94 and 136 GHz	1	Penn Engineering
Transition WR-10 to WR-22	2	Penn Engineering
Transition WR-8 to WR-10	1	Penn Engineering

REFRACTOMETER		
136 GHz, 23 dBm (200 mW) source	1	Millitech
Corrugated Horn antenna - Launching at136 GHz	1	Millitech
Horn antenna - Receiving at 94 and 136 GHz	8	Penn Engineering
High Pass filter - 136HPF (pass 136, reject 94 and 120)	1	Pacific Millimeter
136 GHz detector w/ Video Amplifier	8	Millitech

REFERENCES

[Balanis]

Balanis, Constantine A. (2005) **Antenna Theory.** New Jersey: John Wiley & Sons, Inc.

[Bussard]

Bussard, Robert W. **The Advent of Clean Nuclear Fusion: Superperformance Space Power and Propulson**. Conference Notes from 57th International Astronautical Congress (IAC 2006).

[Bussard]

Bussard, Robert W. **Inherent Characteristics of Fusion Power Systems: Physics, Engineering, and Economics.** Fusion Technology, vol. 26, December 1994.

[Goldsmith]

Goldsmith, Paul F. (1998) **Quasioptical Systems: Gaussian Beam Quasioptical Propagation and Application.** New Jersey: John Wiley & Sons, Inc.

[Krall]

Krall, Nicolas. **The Polywell: A Spherically Convergent Ion Focus Concept.** Fusion Technology, vol. 22, August 1992.

[Pozar]

Pozar, David M. (2005) **Microwave Engineering.** New Jersey: John Wiley & Sons, Inc.

[Swanson]

Swanson, D.G. (2003) **Plasma Waves.** Taylor & Francis, Inc.